REMOTE SENSING

APPLICATIONS IN MARINE SCIENCE PROGRAMS AT VIMS

NASA Wallops Contract NAS 6-1902

Hayden H. Gordon - Principal Investigator

Michael E. Penney - Research Assistant

and

Robert J. Byrne

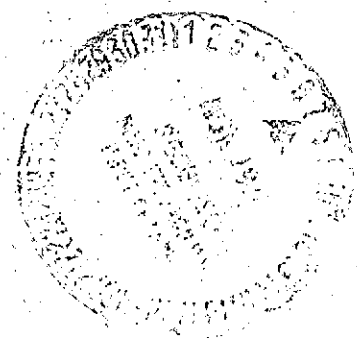

Virginia Institute of Marine Science

Gloucester Point

Virginia 23062

October 1974

Table of Contents

LIST OF FIGURES

ABSTRACT

This report describes ongoing activities performed at the Virginia Institute of Marine Science (VIMS) for NASA Wallops Station to study the applications of remote sensing in marine science. During 1973 scientists at VIMS utilized remote sensing in three programs: tonal variations in imagery of wetlands, use of the thermal infrared to delineate the discharge cooling water at the Virginia Electric and Power Company (VEPCO) nuclear power station on the James River, and the use of aerial photography to determine the volume storage function for water in the marsh-bay complex fed by Wachapreague Inlet on the Eastern Shore of Virginia.

One program was to determine the causes of tonal variations in wetlands imagery and delimit their scope. Results from a predominately single-species salt marsh show variations in tone large enough to cause confusion in an automatic mapping scheme or bioproductivity studies. Film density-bioproductivity correlations for a given sample exhibit variations at different points on the film frame.

Study of the cooling water discharge from the VEPCO nuclear power plant and its effect on the local marine environment is part of a continuing program funded by NASA Wallops and the Atomic Energy Commission. Thermal infrared imagery from a scanner operated by NASA Wallops was used to obtain an instantaneous surface thermal map of the area. Rectification of the strip film from the scanner, thermal-spatial resolution, and the correlation of the geometrically corrected scanner output with ground recorded information is discussed. Some insights into the plume behavior are presented.

Finally, a new application of remote sensing was successfully tested using aerial photography to determine the tidal volumes for various tidal stages within a marsh-lagoon system in a barrier island complex. The capability of black and white infrared film to distinguish a water-land interface was used as a contouring machine to determine the area within the system covered with water, and the volume storage function.

INTRODUCTION

For the past three years the Virginia Institute of Marine Science and NASA Wallops Station have worked together in a program to apply remote sensing in marine science. VIMS has studied the southern Chesapeake Bay and its tributaries extensively over the past twenty years, with most of the data obtained in the field using direct sampling methods. VIMS and NASA have recognized the fact that some of the necessary information can be obtained more easily using remote sensing (and existing fields of study thereby complemented). Several areas of marine research have consequently been investigated for the application of remote sensing. This and two earlier annual contract reports (1971, 1972) detail the progress acheived.

One of the initial programs utilizing remote sensing was the remote detection of oil on water, and a study of oil slick behavior. A great deal was learned using different film and filter combinations as well as the thermal infrared. With most of the experimental releases made in the ocean we believe this work summarized well the best choices available using conventional aerial photography, and the advantages and limitation of the thermal infrared.

A second area where remote sensing has proven valuable is a study of barrier island inlet dynamics conducted on Virginia's Eastern Shore at Wachapreague Inlet. Here remote sensing complemented extensive bathymetry and current recording by giving a plan view of changing surface features.

A new application of remote sensing to barrier island inlet dynamics is presented here. A series of repetitive overflights using

panchromatic infrared film was executed to quantify the water volume storage function of the marsh-bay system fed by the inlet. The method and results of the work are discussed in this report.

The study of tonal variations in wetlands imagery is based upon a phenomenon recognized and studied in agricultural crops. Tonal variations have been shown to cause significant confusion in the interpretation of wetland photography (see Gordon and Penney, 1973), but have not been studied in detail. Analysis this year has focused on determining the magnitude of the variations, and possible correlation with measured plant parameters for a homogeneous salt marsh.

Use of thermal infrared imagery at Hog Point is the continuation of an ongoing program of extensive ground measurements and aerial thermal mapping to delineate volume and surface thermal plume from the Virginia Electric and Power Company (VEPCO) nuclear power plant.

Scientists at VIMS who have utilized the remote sensing available from NASA Wallops have been pleased with the information they have obtained and the extra dimension it has added to ongoing programs. During the past three years of this contract there have been important uses of remote sensing as well as new techniques for obtaining support data. We hope those who read this report and the past two yearly reports will find information of benefit to their ongoing or projected research.

TONAL VARIATIONS IN WETLANDS IMAGERY

Introduction

Even a nonexhaustive review of wetlands research literature reveals at least three types of research problems of management interest: (1) defining wetland-dryland boundaries; (2) mapping and determining areas of species or communities and (3) determining species or community productivities. Egan and Hair (1971), Wobber and Anderson (1972), Gallagher, Reimold and Thompson (1972), and Klemas, Deiber, Bartlett, Crichton and Fornes (1973), have approached the first two problems using various remote sensing media. Analytical techniques have ranged from subjective comparisons of color and tone to automatic densitometry and planimetry. The time consuming nature of interpretive studies is universally recognized and some mention is often made of tonal or reflectance variations as presenting interpretive difficulties. For instance, Egan and Hair determined delimiting tonal ranges for wet and drylands over the film frame for their geographic area. Klemas, et al. point out that "The uniform flatness of marsh topography eliminates variations in reflectance due to sloping surfaces and shadows." Gallagher, et al. recognize, to a degree, that viewing angle changes are akin to topographical angle changes and use the variable illumination in a Kelsh type plotter to balance out tonal variations in conjugate areas of stereo pairs.

Productivity estimates using correlations between measured film densities or reflectances and plant parameters have been mentioned by Gallagher, et al. To date, they have presented only subjective correlations and no detailed quantitative density measurements. Their

feeling that quantitative measurements must always be complemented by some degree of "marsh awareness" or interpretive ability is in some degree supported by this work. Previous work at this institution, Gordon and Penney (1972), has demonstrated that when "marsh awareness" is purposely ignored, tonal variations caused up to forty percent changes in area changes of "plant" or scene types for conjugate areas of the film.

Hoffer, Holmes and Shay (1966), Egbert and Ulaby (1972), Steiner and Haefner (1965), Suits (1972) and Silvestro (1968) have made quantitative and theoretical investigations into the relationships between scene type, tone, reflectance, and viewing geometry. In general, image tone is a complicated, but determinable, function of incident solar flux, angular dependent reflected energy, atmospheric effects, camera radial fall-off function, and film (type and processing effects).

Concerning ourselves only with one mission over a short time, tonal variations are a less complicated function of scene type, radial fall-off, and changes in scene reflectance with viewing geometry. For one scene type, in terms of light reflecting parameters, variations in reflectance or density can be easily determined using procedures detailed by Silvestro (1968). Using these techniques quantitative density or reflectance can be correlated with plant parameters commonly measured by ecologists.

Technique

Field Work

Field work was conducted in a high salinity Spartina alterniflora marsh known to contain three growth forms of Spartina and small

amounts of a Salicornia species. Quarter meter square clip plots were gathered in thirty-three locations predetermined using aerial photographs. An attempt was made to sample all scene types adequately and to place the images at many locations on the composite film frame. The grass samples were analyzed for stem density, length, and diameter then dried and weighed. A summary of measurements for 13 samples used for analysis is presented in Table I.

Histograms for height, weight, stem density, and basal (or total cross-sectional) area revealed that the traditionally recognized growth forms--tall, short and intermediate--are not completely distinguished by these parameters. For instance, "tall" and "short" forms had similar weight and basal area ranges, but different height and stem density ranges. The "intermediate" form intergraded for all parameters.

Remote Sensing Photography

On November 20, 1972, a NASA-Wallops Station remote sensing aircraft (C-54), configured with a T-11 mapping camera (black and white infrared film - 89B filter) and an I^2S four band camera made four passes over the marsh at ~1200 EST (low tide) and four at ~1400 EST (low tide + 2 hours). All runs were at 5,000 feet (scale 1:10,000) altitude. Two additional low altitude passes were made over a set of five different gray panels located adjacent to the marsh and used to facilitate reflectance calculations.

TABLE I

Sample #	Av. Dia. (mm)	Av. Stem Length	Total Dry Wgt. (grams)	# stems	Approx. Basal area (mm^2/plot)
15	3.5	30.8	38.5	134	1146
33	3.0	38.7	31.3	72	509
18	3.8	33.4	25.1	49	556
19	3.6	43.8	75.0	125	1272
25	2.4	29.6	31.4	28	127
11	6.4	90.3	101.4	39	1255
9	9.9	115.1	182.1	22	1693
14	5.2	60.5	47.1	30	1146
24	4.2	47.6	100.2	133	1843
10	2.9[1] 3.2[2]	23.9 20	44.3 56.3	108 252	2739 (combined)
22	5.8	82.6	115.7	54	1427
26	3.0	30.9	71.0	201	1421
28	3.0[1] 5.0[2]	33.6 19	104.6 12.8	204 79	2993 (combined)

[1]Spartina

[2]Salicornia

Calibration

In order to separate density changes caused by the sensor system from those related to the scene and intervening atmosphere it was necessary to calibrate the cameras. To correct the mission film for non-uniform camera transmission effects (which we summarize "radial fall-off") a special calibration source was employed (jointly designed and constructed by Dr. J.D. Oberholtzer and Mr. Charles Vaughn of NASA-Wallops and the authors). The calibration source is, ideally, placed in contact with the camera lens cone (Figure 1) and the camera cycled in the normal manner. Since the source has a uniform energy distribution over an FOV greater than the camera, off-axis tonal changes can be determined. These were found to be radially symmetric for the T-11 (Figure 2) and asymmetric for the I^2S (Figure 3). For the T-11 the relative exposure between the center and an off-axis point is $E(\phi)/E(0)$, where ϕ is polar view angle (PVA)(see Figure 4). Since film density, D, is a logarithmic function of exposure, E, the normalized (to the center) density correction is $\Delta D = D(\phi) - D(o)$. Densities at any point on a mission frame can then be corrected when the PVA of the point is determined. In this experiment, the radial fall-off calibrations were exposed and processed separately from actual mission film. Both pieces of film were normalized to a gamma of one. The asymmetry of the I^2S camera system is unfortunate and may have been caused by extraneous light leaks due to lack of contact between lens cone and calibration source, or flare, which the I^2S occasionally exhibits on normal missions. The asymmetry precluded easy correction of radial fall-off.

Figure 1. Diffuse source for camera calibration.

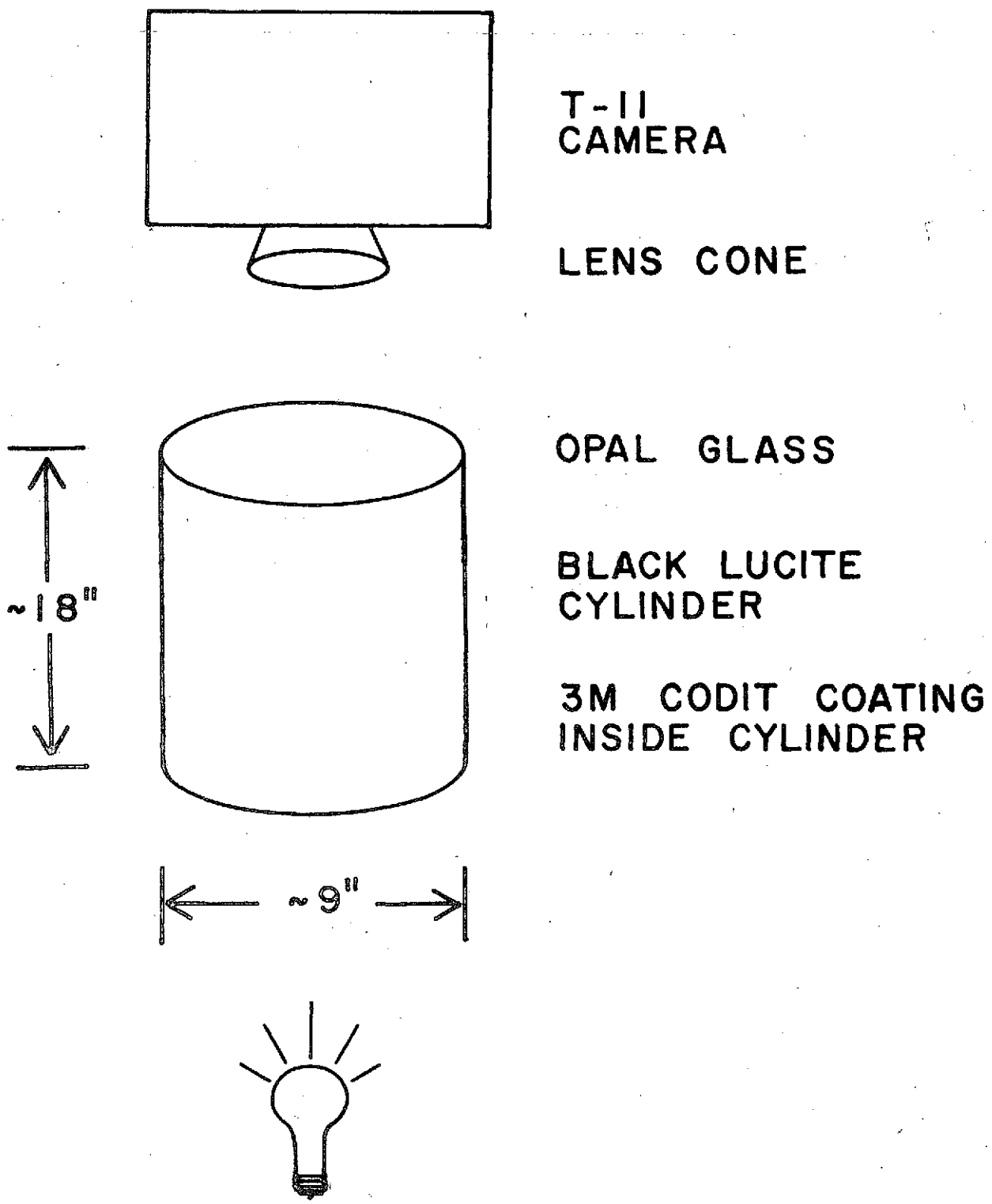

Figure 2. Density correction factors for diffuse calibration of radial fall-off function.

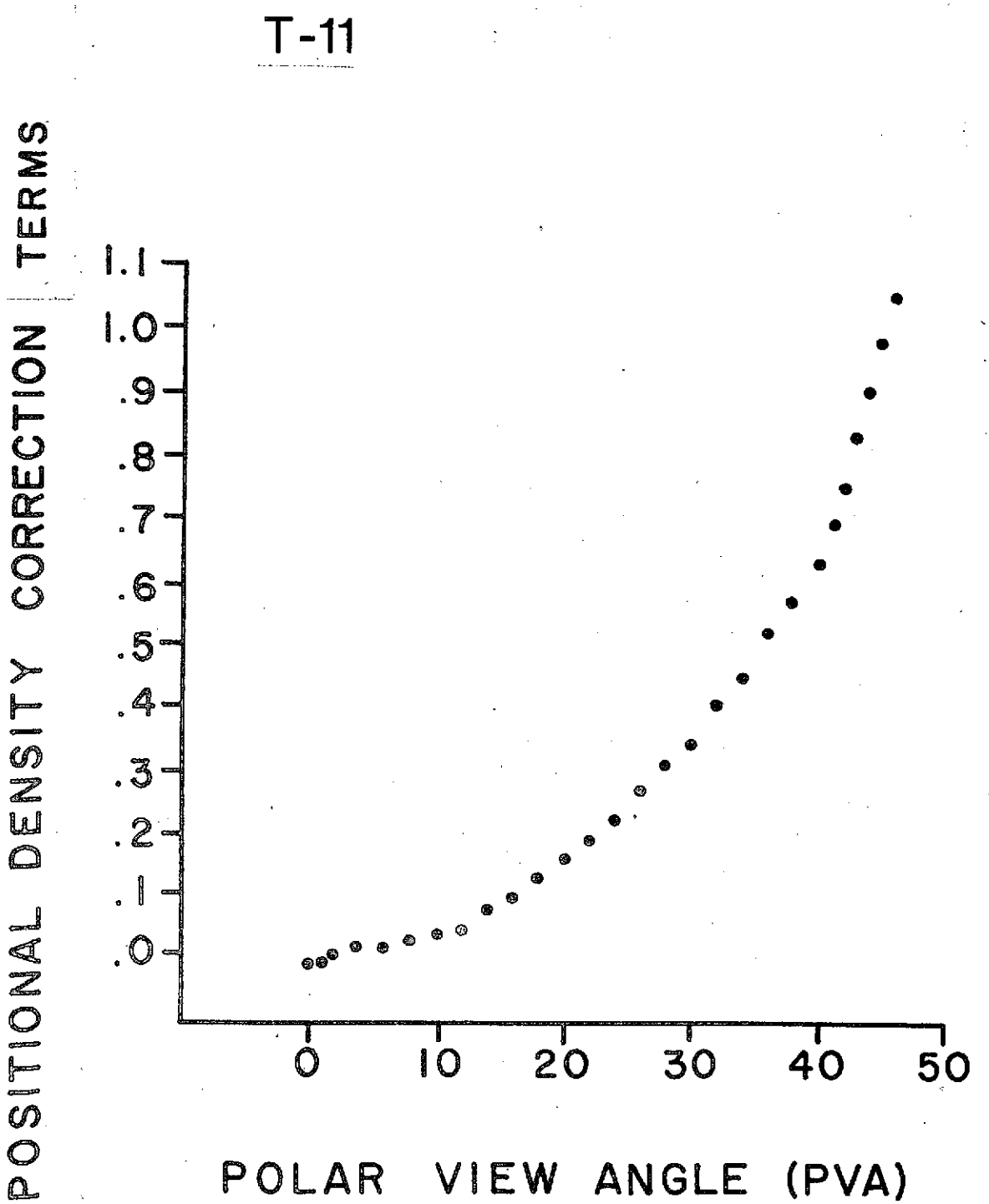

Figure 3. Density values from an I^2S negative exposed with the diffuse source.

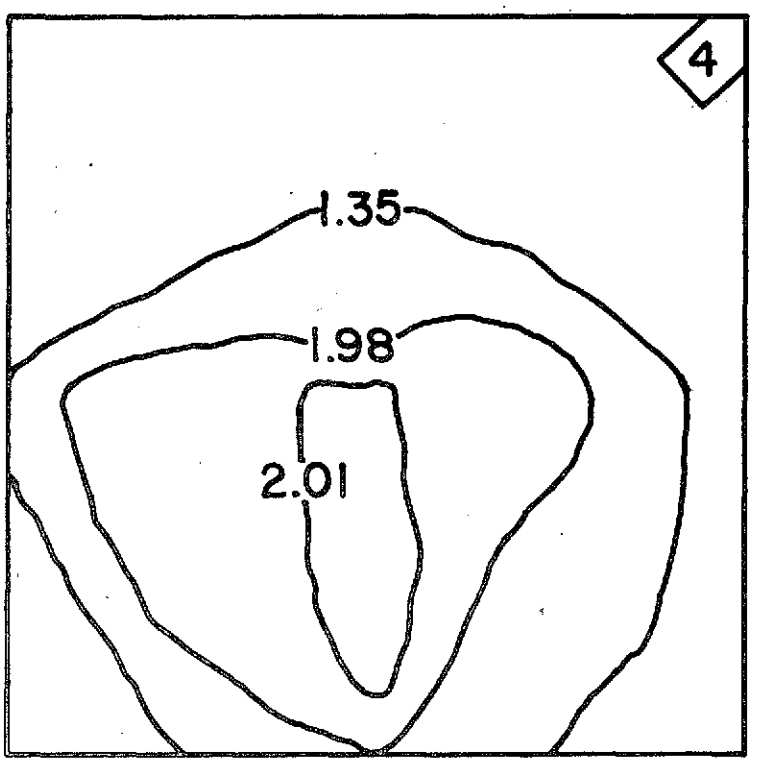

Figure 4. Viewing geometry.

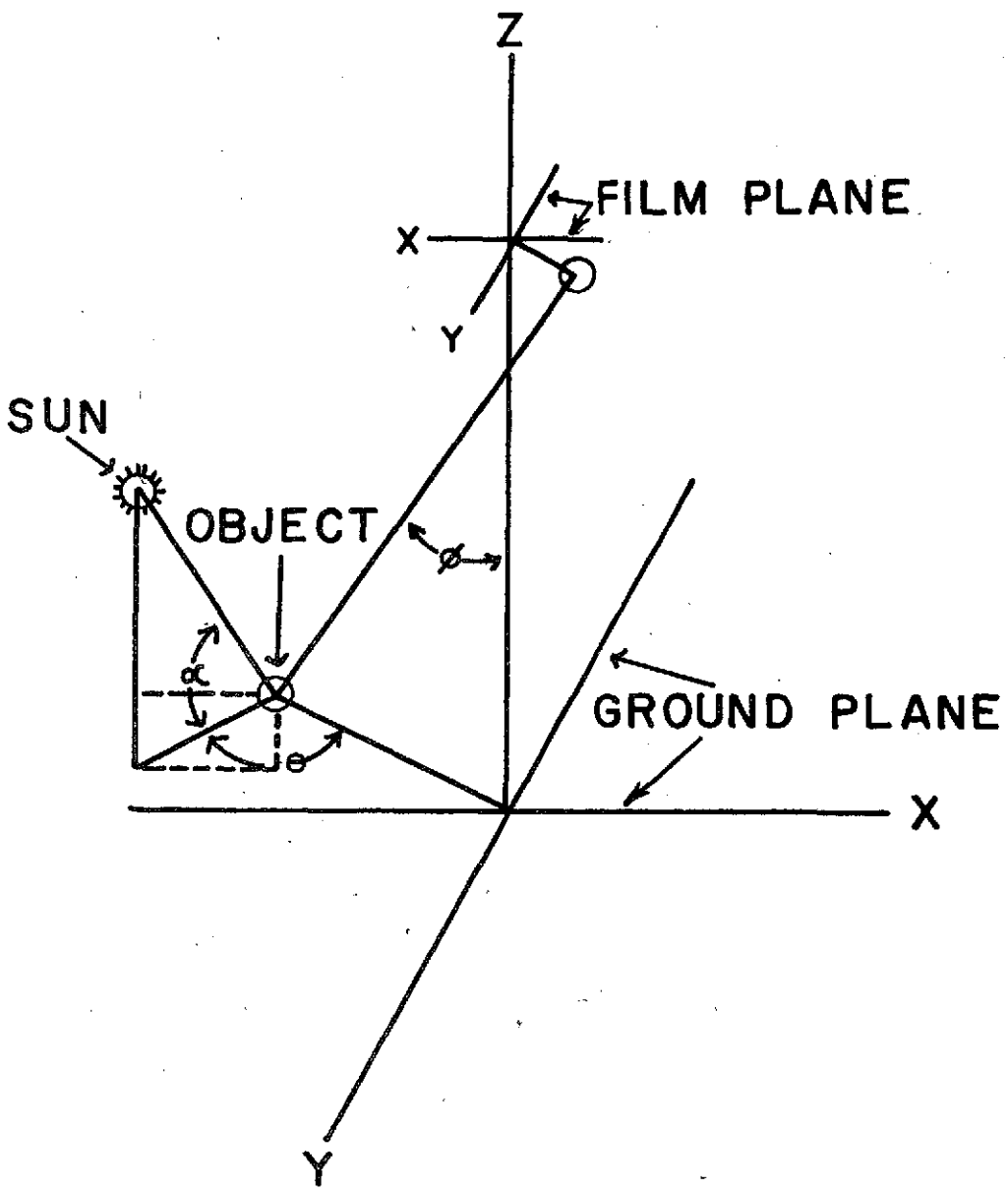

α SOLAR ALTITUDE

$\ominus$ AZIMUTH VIEW ANGLE

$\varnothing$ POLAR VIEW ANGLE

Results

Apositional Analysis

Figure 5 is a smoothed histogram of fall-off corrected mean densities, from a positive, for the three traditional plant types and mud flat from the 1200 EST flight, IR band. Obviously, the three types would be frequently mistaken for each other when viewing geometry and "marsh awareness" are ignored. Plots of mean corrected film density versus stem density (Figure 6), height (Figure 7), weight (Figure 8), basal area at 1200 EST (Figure 9), and 1400 EST (Figure 10) show no obvious functional relationships (numbers refer to Table I samples). For example, images (of plant samples) having a contrast of approximately 0.2 density units at all (present) film positions were found to occupy overlapping stem density, height, and weight ranges. So, if viewing geometry had been ignored, a contradicting, false interpretation would have been made about film density parameter correlations. Basal area, which is inversely proportional to the soil visible, gives much less contradictory results, even ignoring viewing geometry. Above a basal area of approximately 1400 mm^2/plot there is a sharp drop in mean film density (or increase in reflectance--see appendix). This density or reflectance change is significant at the 10% level (two sample t test) if the groups greater and less than 1400 mm^2/plot are compared. The density difference is less startling, though still significant at the 10% level, on the 1400 EST flight for reasons not presently clear to us, but probably involving a change in the geometry dependent reflectance function at the lower sun angle. Complete analysis of such an effect requires a more extensive sampling program with different basal area groups moving through the same point loci.

Figure 5. Film density histogram.

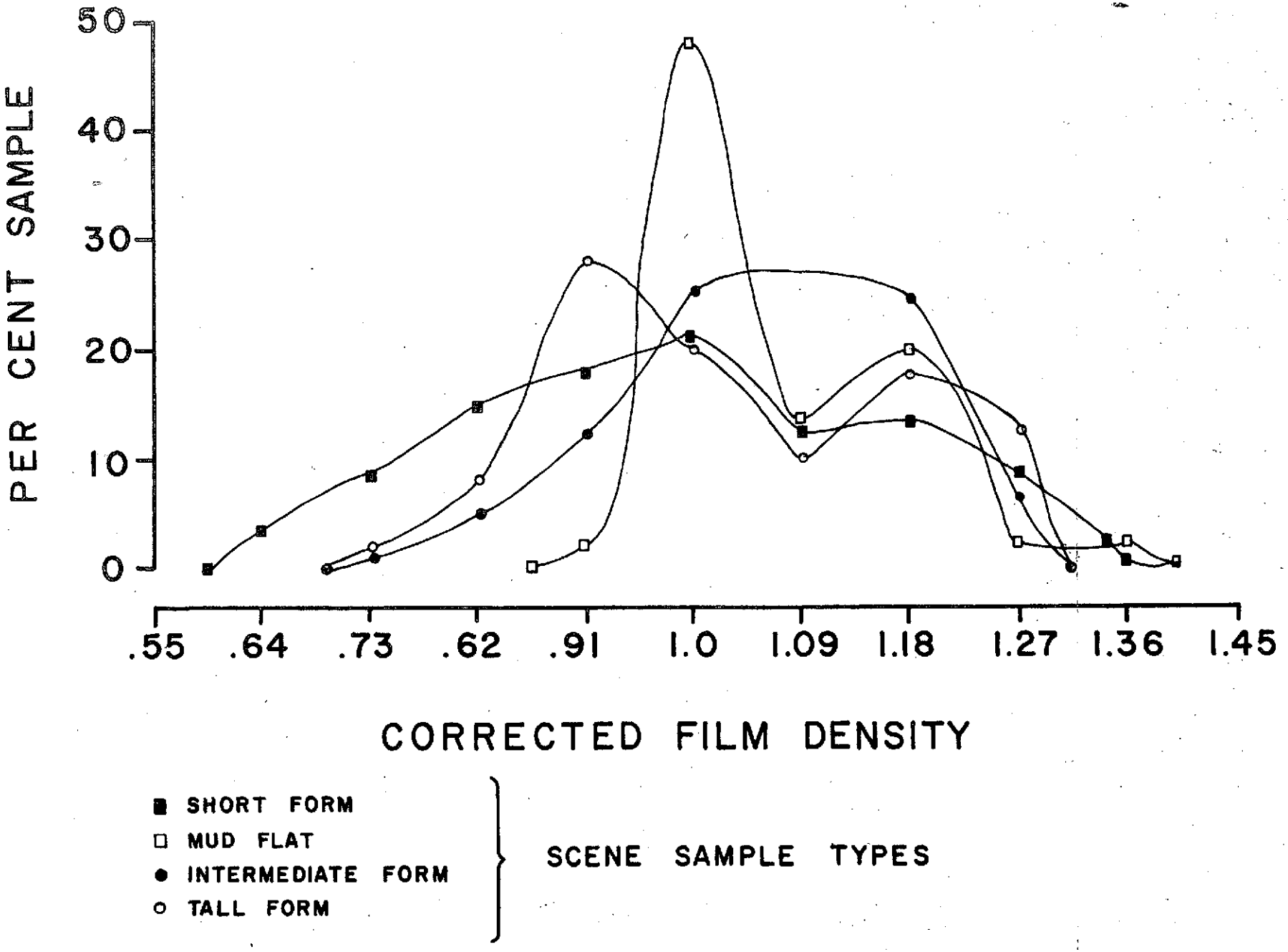

Figure 6. Corrected mean film density vs. stem density T-11 IR band (~1200 EST).

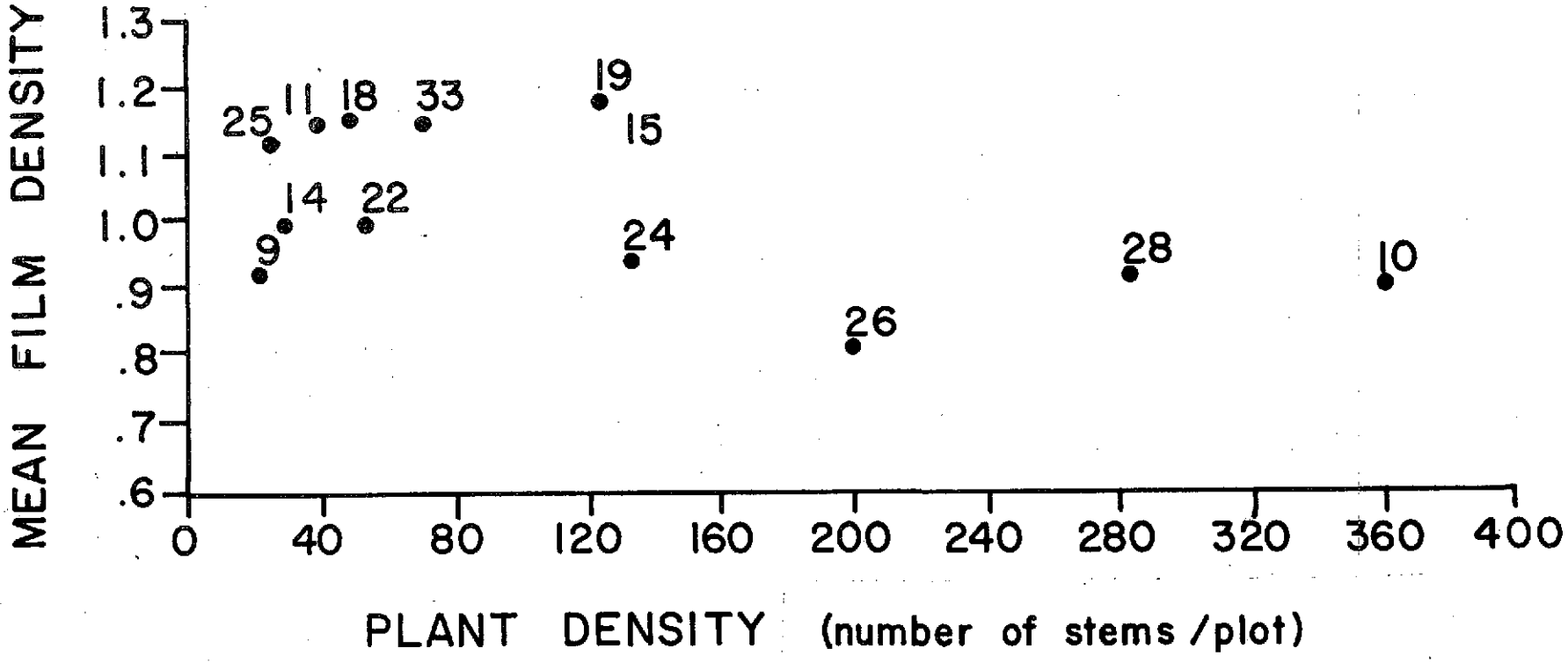

Figure 7. Corrected mean density vs. height T-11 IR band (~1200 EST).

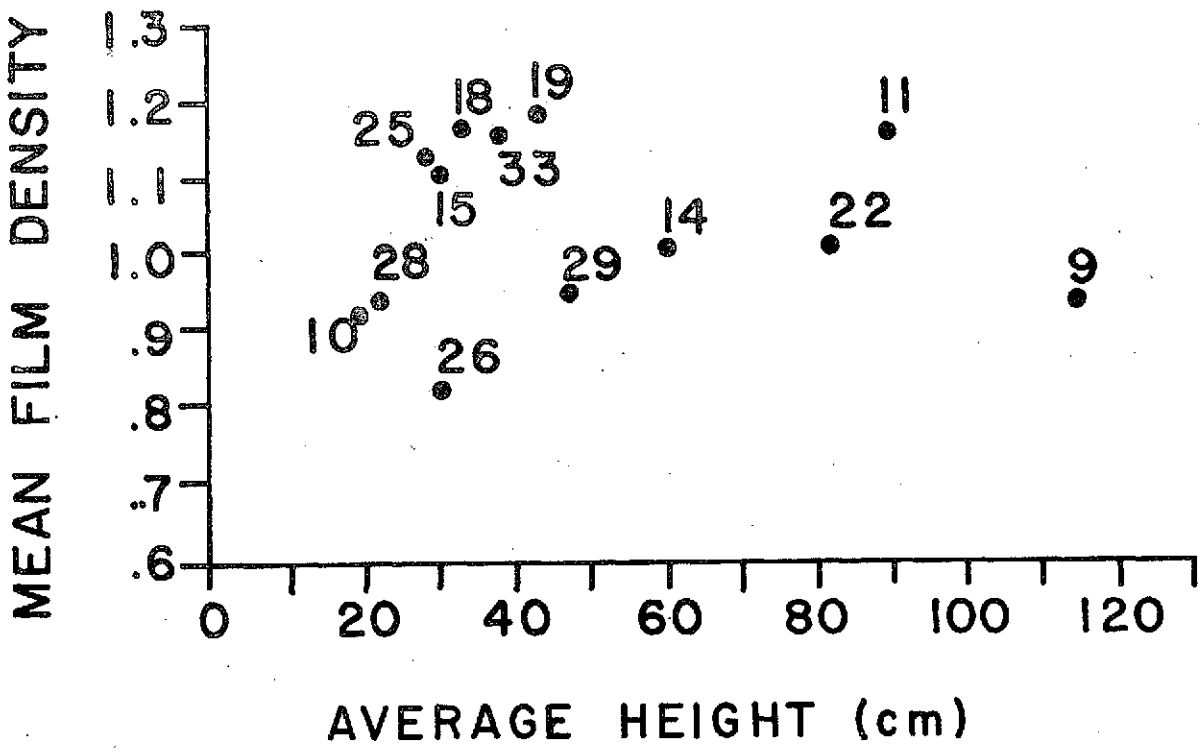

Figure 8. Corrected mean density vs. weight T-11 IR band (~1200 EST).

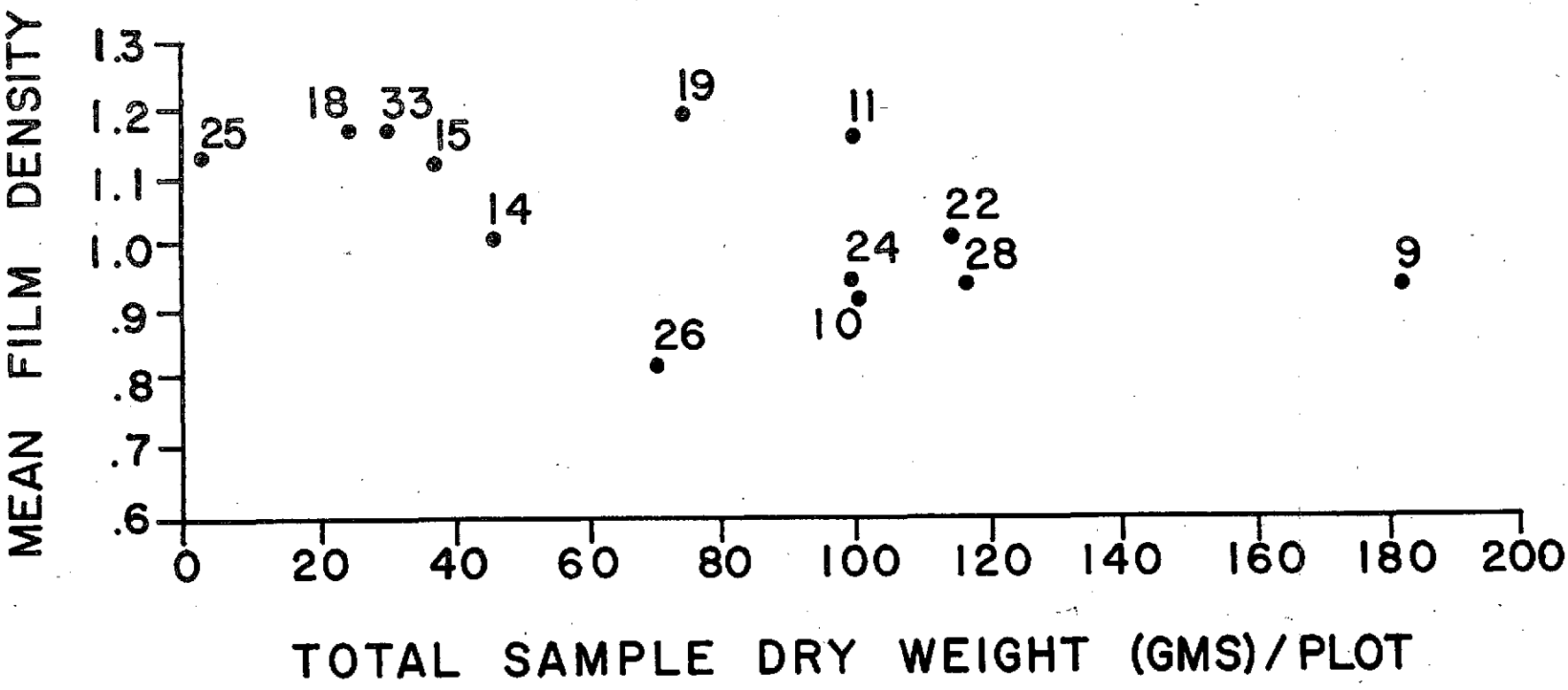

Figure 9. Mean film density vs. basal area plot T-11 IR band (~1200 EST).

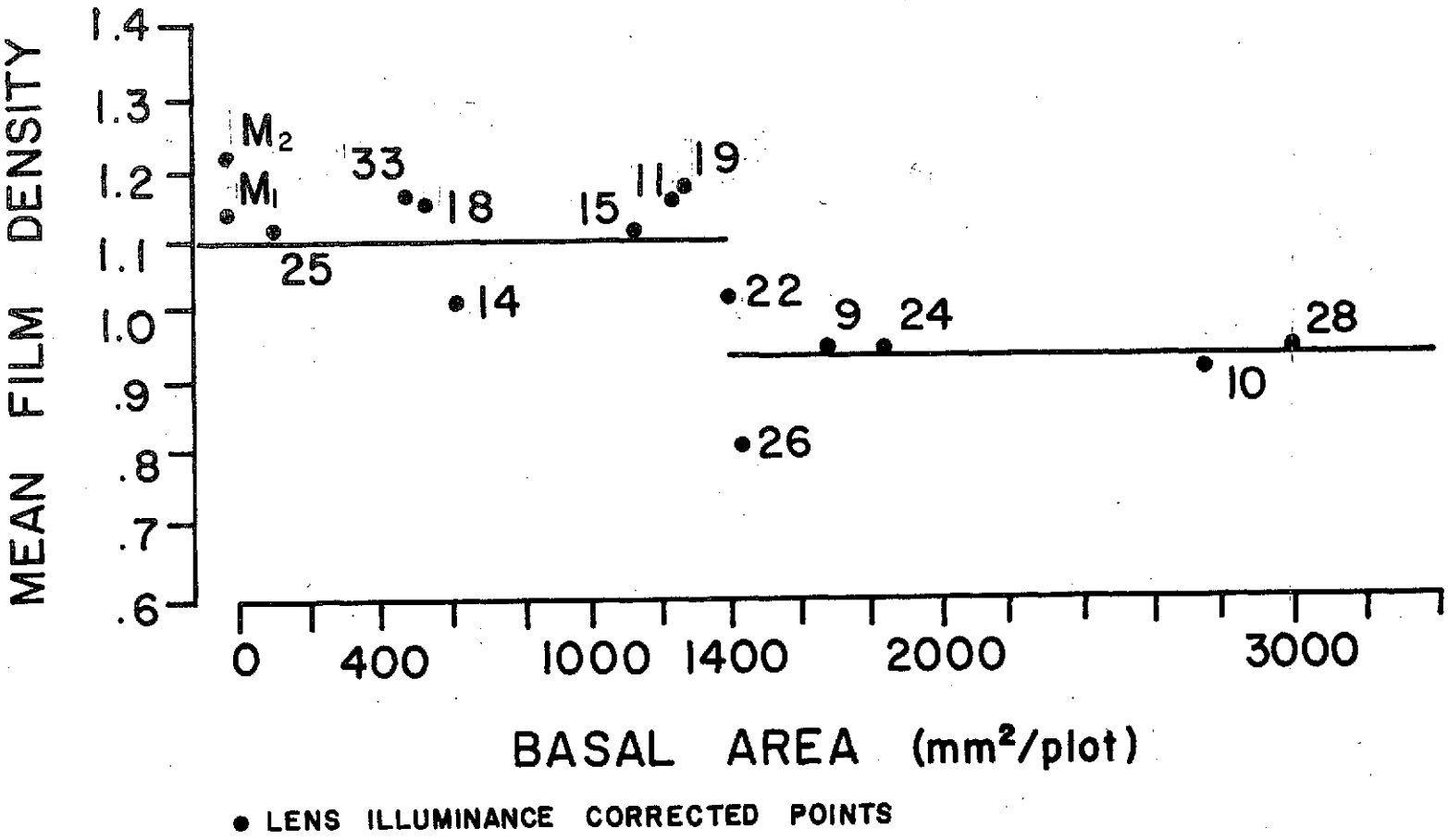

Figure 10. Corrected mean film density vs. basal area T-11 IR band (1400 EST).

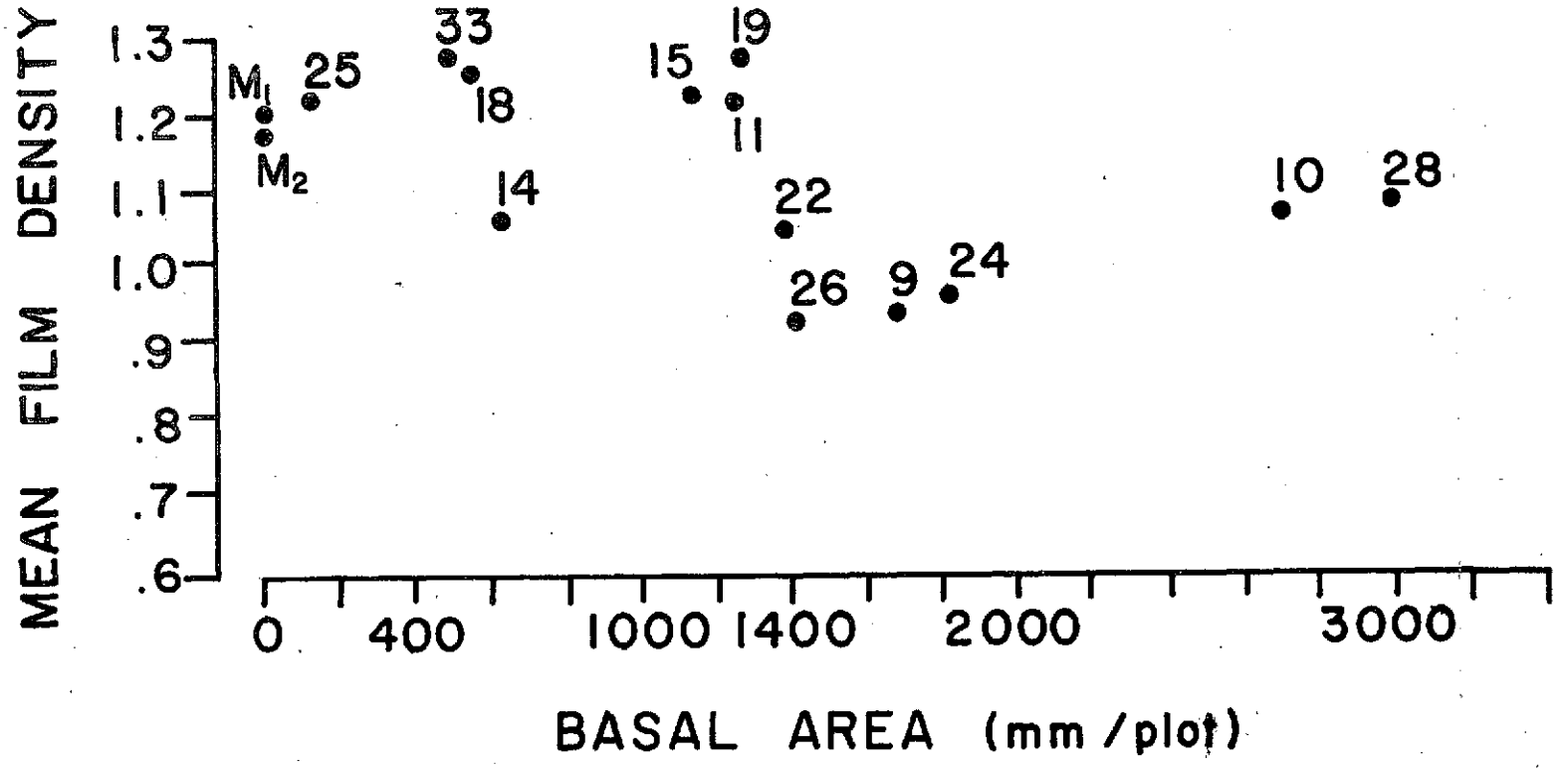

Positional Analysis

Figures 11, 12, 13 and 14 are various ways of presenting density data positionally. The isoline plots in 11 and 12, contoured by someone unfamiliar with tonal variation concepts, are for the $<1400\ mm^2$/plot group. The patterns are similar for the two flights, having slightly greater rates of density change on the northerly side of the frame (or sun azimuth line) than the southerly side. East-west differences may be indicative of some real functions of viewing geometry, or simply, sampling inadequacies. Further work in this type of marsh could lead to generation of a reliable density correction mask for view angle effects. Ideally, a mask for each of the important marsh species would make productivity mapping more accurate and help identify viewing geometry regions in which species discrimination would be more accurate.

Figure 13 presents the $<1400\ mm^2$/plot with the composite film frame divided into columns perpendicular to the flight line (and point loci). This approach divides the total sample into two azimuthal groups. Points between 0° to 90° AVA and 270° to 0° AVA are one group. Points 90° to 270° are the other. Column -4 to +4 represent equidistant divisions of a sample point locus from its first entry into the frame to its exit point. Column 0 is the closest approach to the frame center. It is interesting that between group contrast changes slightly over the frame, but, as in the isoline presentation, rate of density change appears to be greatest on the north side of the frame. The area in black is the overlap of the one standard deviation units for each group by column. Variability in this overlap may be due to sampling

Figure 11. Contoured composite photo for samples < 1400 mm²/plot (~1200 EST).

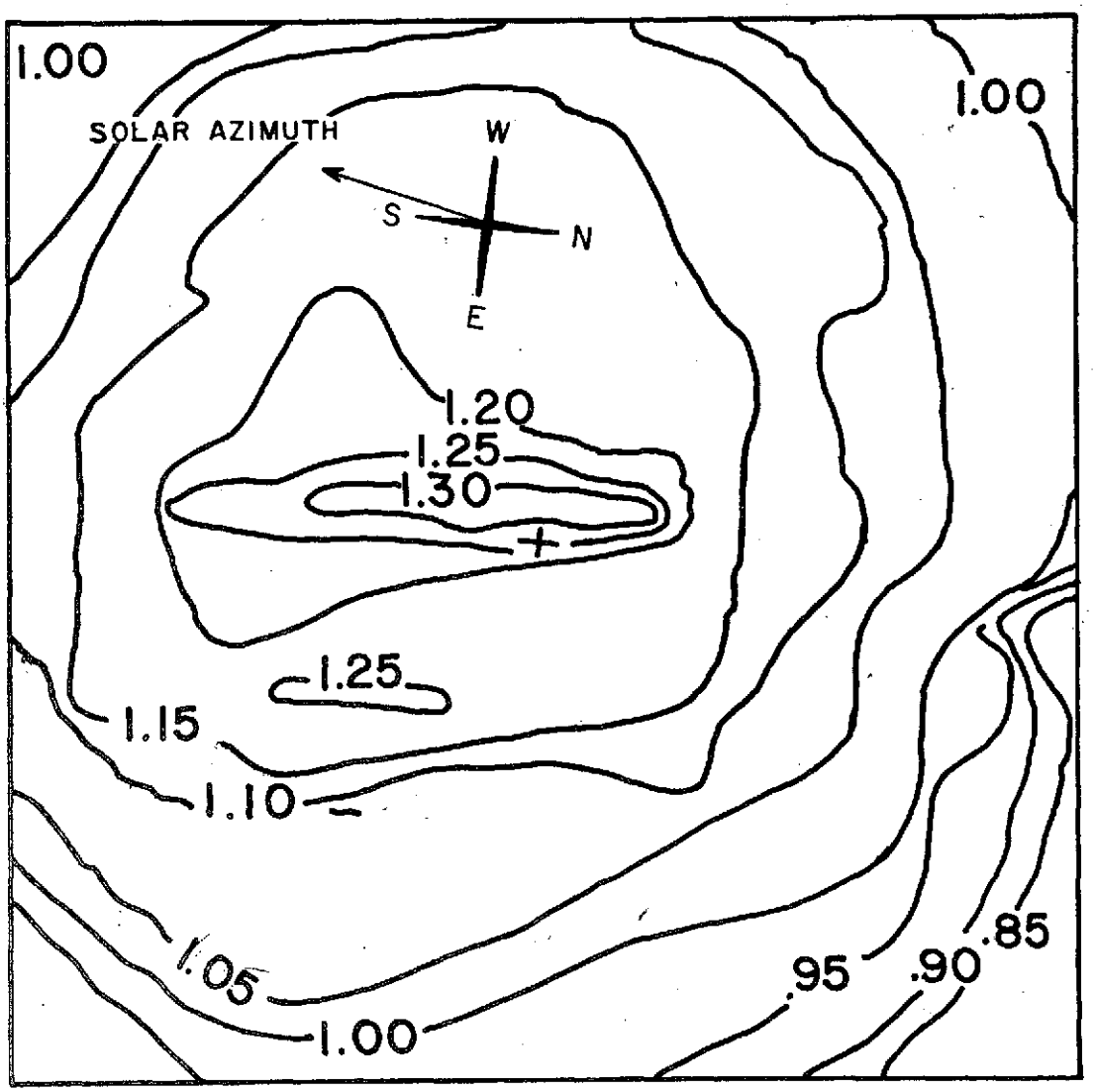

APPROXIMATE SOLAR AZIMUTH SHOWN

SOLAR ALTITUDE ~ 37°

Figure 12. Contoured composite photo for samples < 1400 mm²/plot (~1400 EST).

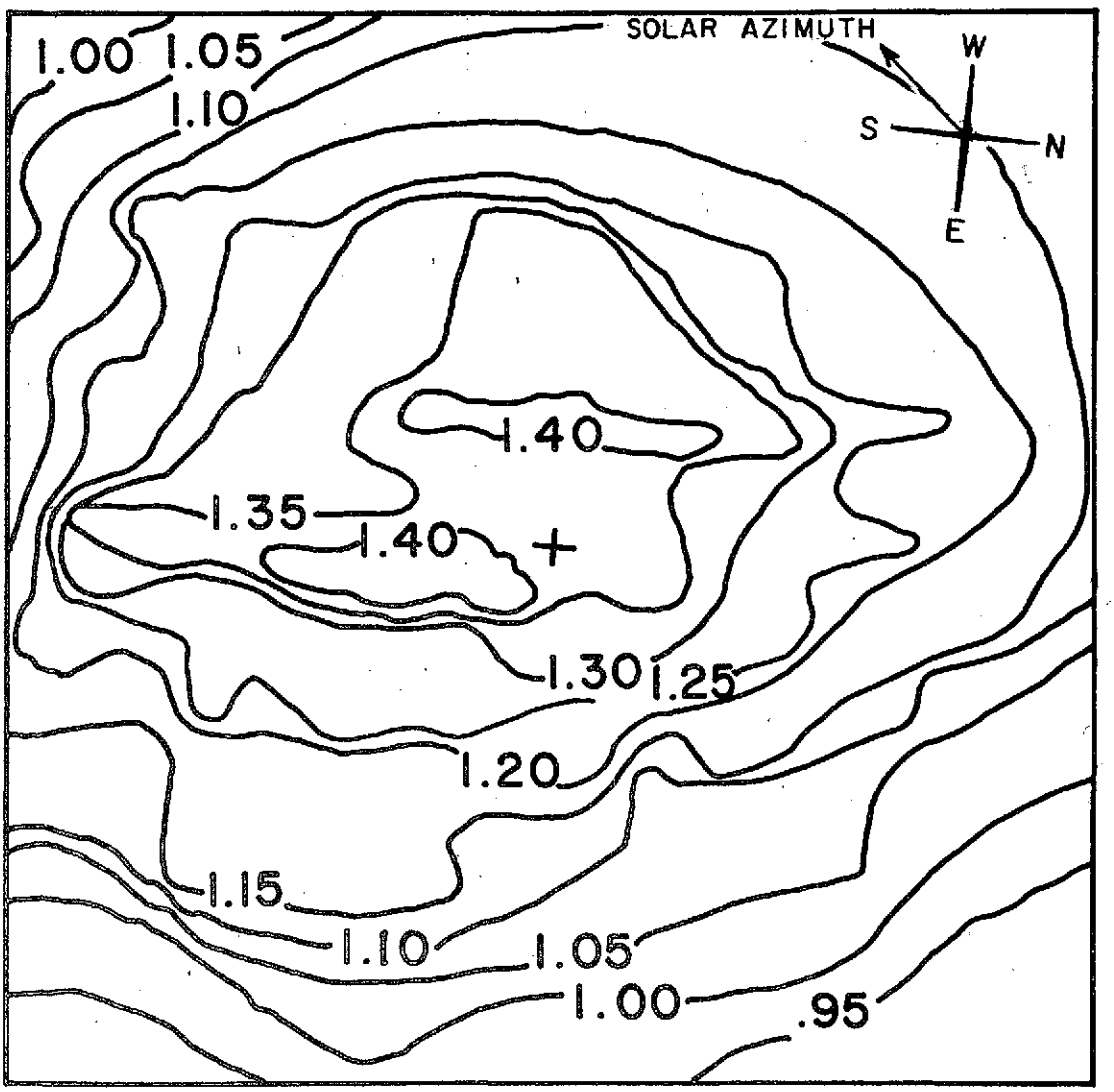

APPROXIMATE SOLAR AZIMUTH SHOWN

SOLAR ALTITUDE ~ 20°

Figure 13. Composite frame points grouped by columns perpendicular to flight line.

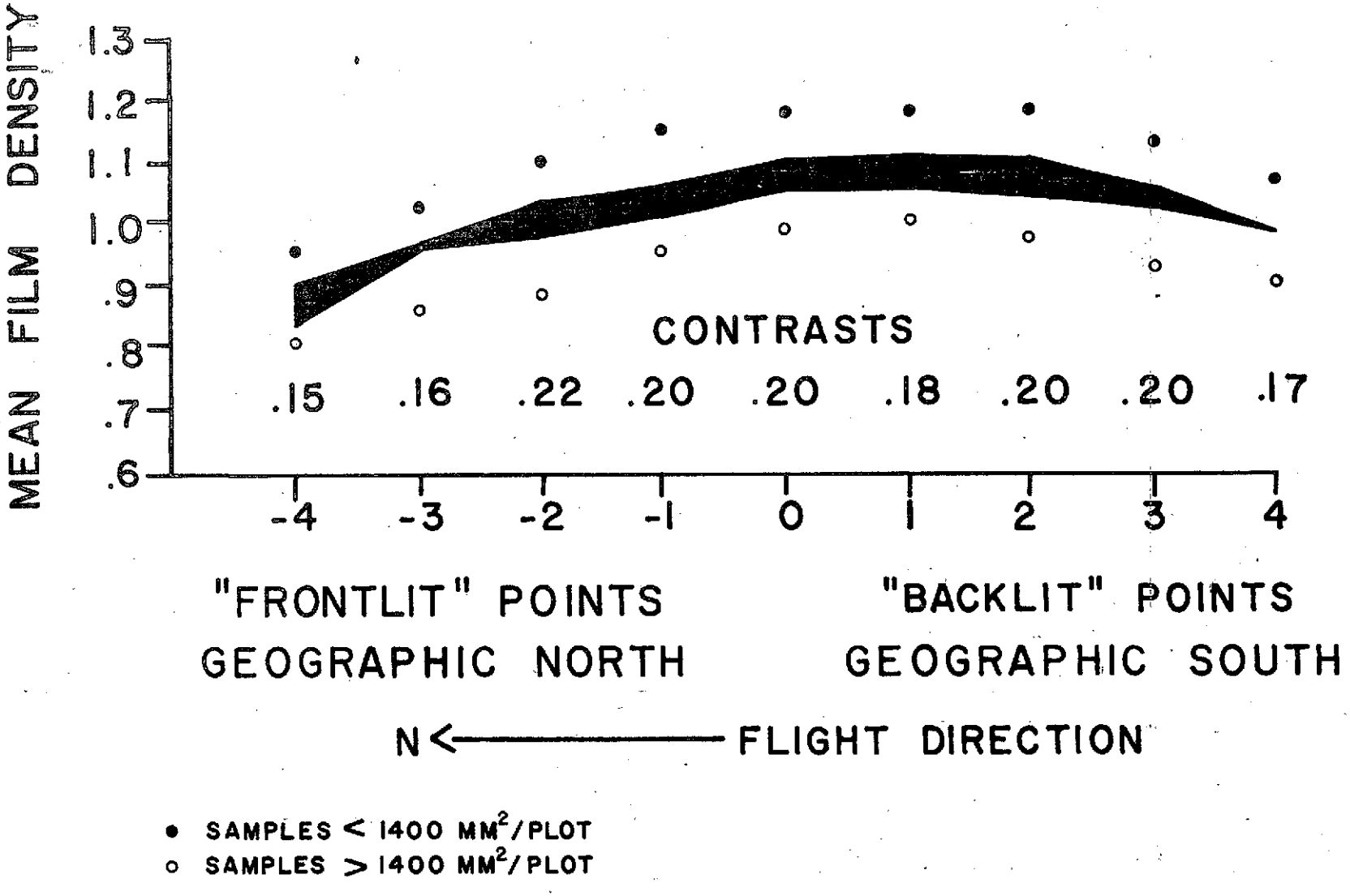

deficiencies. Figure 14 is the composite frame divided into polar view angle annuli. Differences in contrast and standard deviation overlap may again be sampling deficiencies. Essentially, the column approach ignores polar view angle and the polar view angle approach ignores azimuthal view angle.

An analysis of variance would require different sampling, but it seems clear that "frontlit" samples have higher reflectance than "backlit", and that reflectance increases (density decreases on a positive) with increasing polar view angle. Both conclusions are supported by work in agricultural remote sensing literature.

Raw-Corrected Data

Figure 9, from T-11 data, basal area at 1200 EST, compares fall-off corrected and uncorrected data. It is important to note that the reflectance increase at 1400 mm^2/plot would not have been visually noticed in the uncorrected data.plot. In fact, a two sample t test on the raw data for greater than 1400 mm^2/plot and less than 1400 mm^2/plot sample groupings is not significant at the 10% level. The mean T-11 corrections were used on the I^2S red and green band data, making the very risky assumption that the I^2S fall-off is indeed symmetrical and of the same general shape as the T-11. Figures 15 and 16 show red and green band raw and corrected densities plotted with basal area. Possible fitted lines are shown with dashes. The data is suggestive of no correlation in the red and slight correlation in the green. These differences between raw and corrected data imply that caution must be used when interpreting quantitative, but uncorrected, data.

Figure 14. Composite frame points grouped in polar view angle annuli.

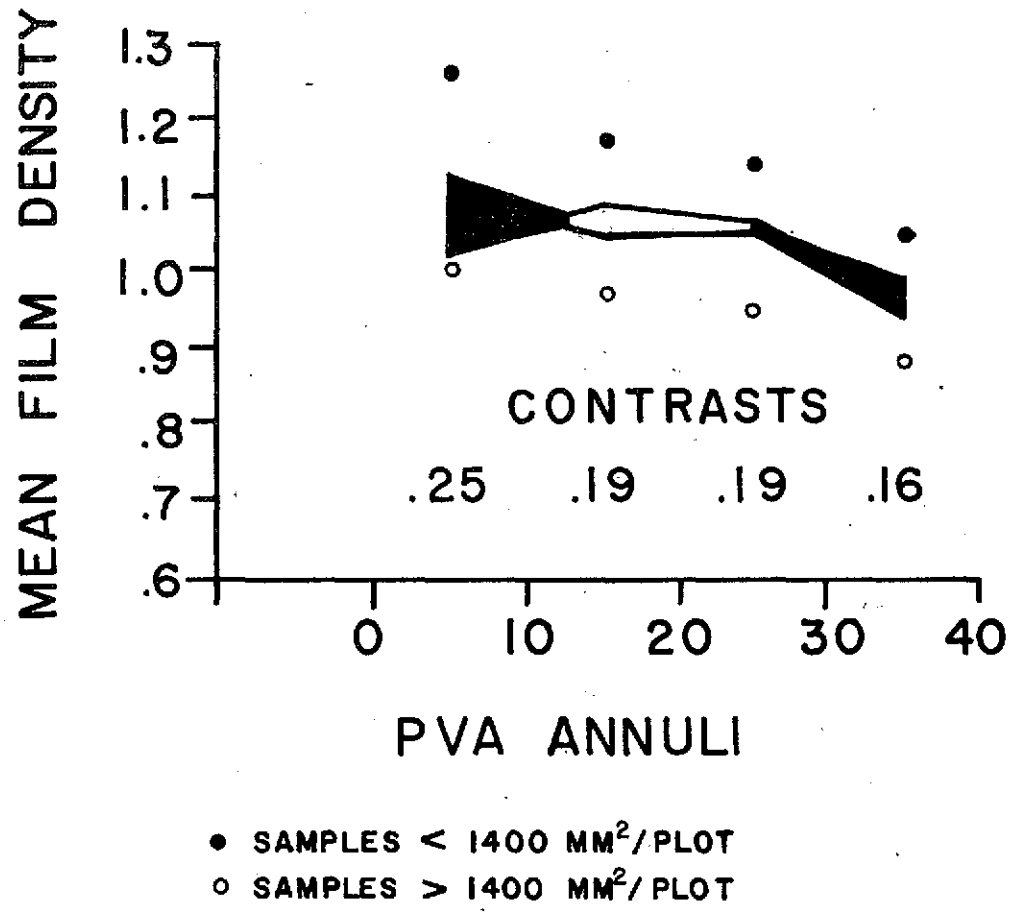

Figure 15. Mean film density - raw & "corrected" - basal area I^3S red band (~1200 EST).

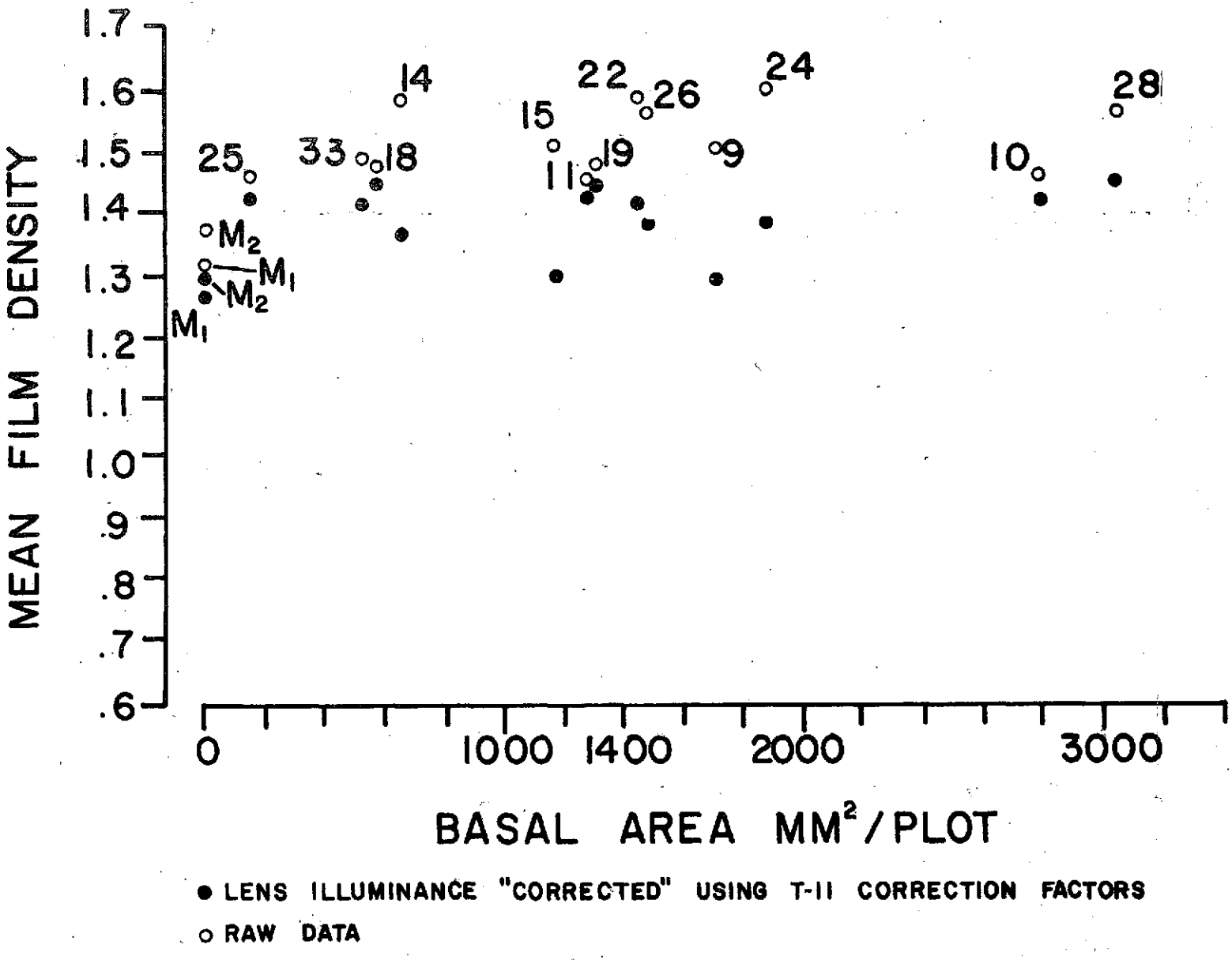

Figure 16. Mean film density, raw & "corrected" - basal area I²S green band (~1200 EST).

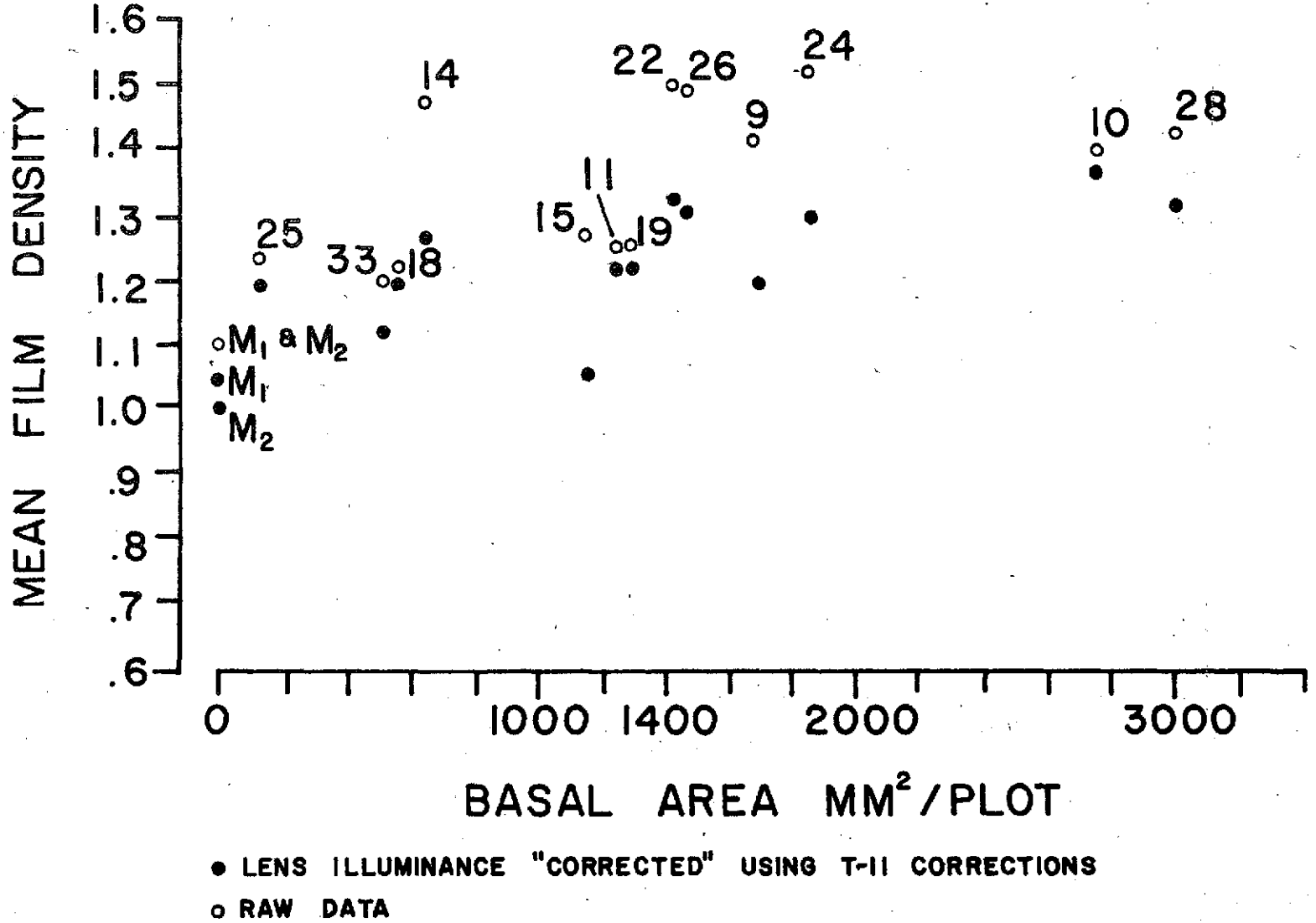

Reflectances

It is possible, following Silvestro's method (1968) to calculate reflectance of scenes from corrected densities. Film exposure on the negative is proportional to reflectance in an equation of the form

$$E(\lambda) = \alpha(\lambda)\, r(\lambda) + B(\lambda)$$

where $\alpha(\lambda)$ is a constant (over the exposure time but dependent on solar flux) and $B(\lambda)$ is that energy from atmospheric scattering added to the imaging light. In our case λ represents the 0.7 - 0.9 micrometer band (B & W IR). Three such equations of this sort were written for two ground panels of known reflectance as well as for the scene. Solving the three equations for target reflectance, $r_x(\lambda)$, the following is obtained:

$$r_x(\lambda) = \frac{[E_x(\lambda) - E_B(\lambda)]\, r_w(\lambda) + [E_w(\lambda) - E_x(\lambda)]\, r_B(\lambda)}{E_w(\lambda) - E_B(\lambda)}$$

where E_w, r_w, E_B, r_B are exposure and reflectance for the white and black ground panels, respectively.

Reflectance data for the IR band is presented in the appendix. Plotted with plant parameters, reflectance showed essentially the same behavior as mean corrected densities. The 1400 mm^2/plot discontinuity was still evident.

Conclusion

It seems clear why, when marsh awareness is ignored, subjective color or tone keys can prove inconsistent or ineffective. Film density in all bands varies due to lens illuminance (radial) fall-off,

and scene viewing geometry. On a positive, with increasing polar viewing angle, marsh scene reflectance increases and therefore density decreases. Lens illuminance fall-off has the opposite, in a sense, partially balancing effect. As a result of these opposite trends in density change, use of an anti-vignetting filter causes tonal variations due to salt marsh scene viewing geometry to be more visually noticeable. Analysis of some six hundred density measurements presented here showed that "raw" illuminance corrected measurements can give different results when plotted with various plant parameters. Plant samples at the extreme ends of the height, standing crop biomass, and stem density ranges often had closely similar mean (corrected or raw) film densities. For this data set, there was a statistically significant change in mean corrected film density at a basal area of $\sim$1400 mm^2/quarter meter^2 sample plot. Further work, in progress, may or may not make this conclusion generally applicable for this type of marsh community. However, the implication is that in the near IR band reflectance is not as dependent on biomass, stem density, or height as it is on amount of soil visible.

Reflectance (or density) plant parameter correlations will continue to be investigated by the authors. An attempt is being made to compare only samples having the same viewing geometry. Use of color IR film will speed multiband data analysis by eliminating the need to locate each image point more than once in the densitometer. Ground panels and densitometry will continue to be used, and fall-off calibrations will be performed on the mission film to eliminate gamma normalization between films.

HOG POINT THERMAL STUDIES

Introduction

Thermal studies of the James River in the vicinity of the Virginia Electric and Power Company (VEPCO) nuclear power generating plant (Surry County, Virginia) have continued during 1973. The work done by VIMS under contract to the Atomic Energy Commission (AEC) and NASA Wallops this past year has been directed toward monitoring the immediate section of the river near Hog Point throughout the initial period of operation of the power plant. The background conditions of the environment have been studied during 1971 and 1972 with an instrumented boat, *in situ* tower, and airborne thermal scanner (see Bolus, *et al.*, 1971; Shearls, *et al.*, 1973; Gordon and Penney, 1972).

Research under the NASA Wallops contract has been directed toward the use of the thermal infrared, its interpretation, and application to the problem of mapping the temperature structure in a time dependant estuary. Described in this section of the report are the scheme used for rectification of the infrared imagery, determining the resolution of the scanner, and results of a thermal flight during high slack tide and the beginning of ebb flow in the outfall vicinity of the James River with the nuclear power plant in operation.

Thermal-Spatial Resolution

In order to locate discrete positions on the infrared scanner film record such as the instrumented boat or the data acquisition tower it is necessary to have an object which emits either more or less energy than the surrounding water and is within the spatial

resolution capability of the scanner. From past experience it was found that the 30 foot instrumented boat could not be located on the film at the working altitude of 2,000 feet. An experiment was devised to run concurrently with an actual data flight in the field. To get an order of magnitude measurement of the thermal-spatial resolution, overflights were requested at 500, 1,000, 2,000 and 5,000 feet altitudes over a boat anchored at the tower with a special infrared target. To make the target two sheets of masonite (½" x 4' x 4') were painted silver on one side (low emissivity) and flat black on the other side (high emissivity). The energy source was the sun and the panels were oriented during the day to form a 4' x 4' & 8' blackbody (both large and small emissivity). A small hole was drilled in the edge at each panel to accept a special thermistor for measuring the internal temperature. Figure 17 is an unsmoothed plot of the temperature variation for each configuration. The fluctuation in values, especially noted in the black panels, was due to interruption of sunlight by clouds. Between 1500 and 1600 hours the sun was completely obscured and the black panel reached an equilibrium temperature of 20-21°C from indirect radiation. Results of the experiment are summarized below in Table II.

Table II

Altitude	Black 4 x 8	Silver 4 x 8	Black 4 x 4
.5 K	V	V	V
1 K	V	M	M
2 K	M	N	N
5 K	N	N	N

V - visible, M - marginal, N - not visible

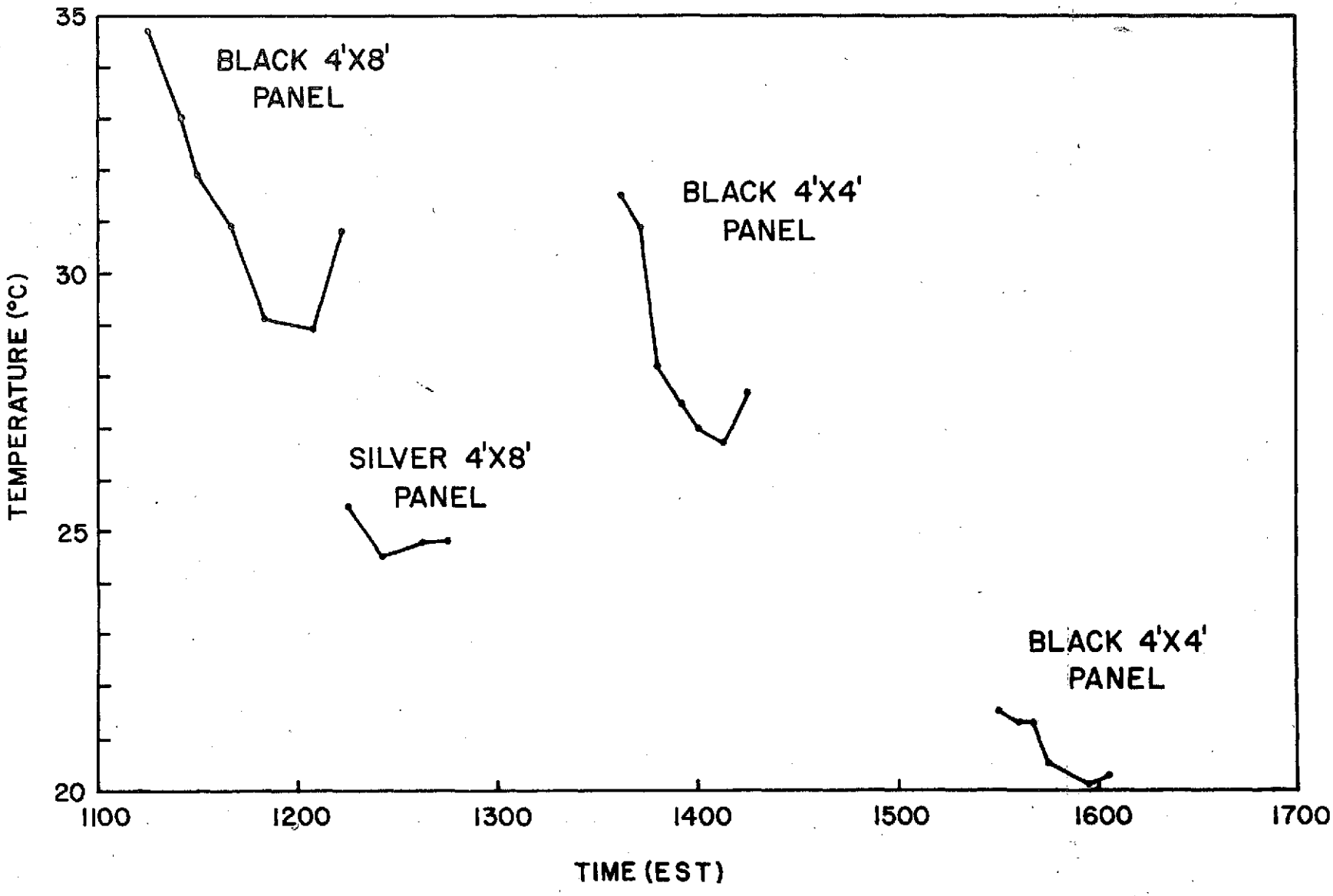

Figure 17. Temperature vs. time for experimental test panels.

To be classed as visible an observer must be able to recognize the image on the scanner film placed on a light table with no magnification. Use of this type of marker system is, therefore, not feasible for work done at altitudes greater than 1,000 feet. A suggestion we would like to try during the course of next year's experiments is use of a charcoal brazier in a floating platform (H. Jones, Photo Science, Inc., personal communication). Although spatially smaller than one of our panels, the charcoal at its very high temperature should radiate enough energy to image as a discrete spot on the scanner film.

Geometric Rectification of IR Scanner Film

The utility of strip film from an infrared scanner is greatly reduced if features which are thermally imaged cannot be put into proper perspective and correlated with other sources of information. The problem of geometric distortion is particularly acute over water where there are relatively few stationary features to help orient the thermal image and remove the inherent distortion. Causes and manifestations of distortion in IR strip imagery are discussed in articles by Sabins (1973) and Masry and Gibbons (1973). In order to use the imagery to outline the thermal plume in its proper perspective the progressive compression of information toward the film edges caused by constant angular scanning and linear recording must be eliminated. One method of accomplishing this is to use the film's center portion of roughly 40° coverage where distortion is minimal, and by flying parallel lines to gain the desired lateral coverage. Reconstructing the overlapping strips becomes very difficult over water, however, for

reasons stated above. Another solution is to reduce the scale of the imagery, thereby confining the area of interest to the central portion of the strip. This is possible only to the point where too much information from the scene is lost through the atmosphere. As a result of experimentation, 2,000 feet was chosen as an optimum altitude for recording the maximum amount of information at the smallest scale over the Hog Point site.

At an altitude of 2,000 feet the thermal plume is generally confined to one strip width flown such that the shoreline is at the very edge of the film format. In this situation rectification is needed to accurately locate the plume and determine its true shape. In order to accomplish this a simple mapping transformation was employed. A rectangular grid was used to overlay the scanner film and a special grid with progressively wider spaced lines in the cross-track dimension (symmetrical about the nadir) was drawn. A point by point transfer of features of interest from the film to the special grid served to "undistort" the scanner imagery. The method was tested using imagery flown east-west over Hog Point at the power plant site and linear features such as roads and power line clearings were checked against a recent map of the area made from aerial photography. Correlation was in general good although there was some misplacement of features caused by aircraft crab, altitude change over the run, and speed variation. Still, agreement with the base map was better than 10% (displacement of known features from their true location).

An improvement of the rectification scheme, to be tried next year, will rely on automation. Imagery will be digitized on the NASA Wallops scanning microdensitometer, the rectification performed on the magnetic tape with computer processing, and the resulting information used on the same densitometer to expose a new piece of film. The new film will contain the original radiometric information relatively free of geometric distortion.

Thermal Flight 4/17/73

On April 17, 1973 the NASA Wallops C54 equipped with the AAD-2 infrared scanner and a T-11 mapping camera (S0397 color film) made repetitive flights over the VEPCO nuclear power plant discharge jetty and adjoining section of the James River. Ground truth during this period was gathered from the instrumented boat running transects, a second boat anchored at tower #6, and some instrumentation on the tower itself. Measurements made by the moving boat were water temperature at 0.5, 3 and 6 feet below the surface, air temperature at 3 and 6 feet above the surface, dew point temperature, and salinity. The second boat, in radio communication with the aircraft, recorded water temperature during the day at the 0.5 foot depth (as well as performing the spatial-temperature resolution experiment). Since the Braincon data acquisition system was not installed on the tower, wind velocity only was recorded.

The aircraft made four groups of passes over the area beginning at 1040, 1200, 1330, 1530 EST. Each group consisted of three passes perpendicular to the discharge shoreline (center line over the power

plant plus one line on either side) at 500 feet altitude, and four passes parallel to the shoreline and directly over tower #6 and the stationary boat at altitudes of 500, 1,000, 2,000, 5,000 feet. The instrumented boat began its run on transect #4 (T4) at 1102 EST and completed a partial run through transect #8 (T8) at 1211 EST. Engine trouble precluded making an entire run or repeating the transects as had originally been planned. The stationary boat was put on location at the tower in the morning (1000 EST) and remained until 1600 when the aircraft made its last pass. Before returning to the dock the boat took a final temperature reading approximately 100 feet outside the discharge jetty.

As a background for the following discussion Table III is included to summarize the status of factors important to the plume behavior. Figures 18, 19, 20, and 21 show the rectified thermal plume outline on a map of Hog Point. All four are to the same scale and each made from one strip of scanner imagery flown from north to south at 2,000 feet altitude parallel to shore and directly over tower #6. Figure 22 is a composite made from four of the original 70 mm scanner strips taken at 1140, 1240, 1440, and 1600 EST. The two dark lines running longitudinally either side of the center are artifacts caused by the recording process and should not be interpreted as a part of the scene. Figures 18 and 19 show the transects followed by the instrumented boat. The temperature contours are drawn from the data taken by the boat at the 0.5 foot depth. Refer to Appendix B for the original data recorded by the boat on April 17. Figures 20 and 21 have no boat transects or temperature contours since the overflights were made after the boat

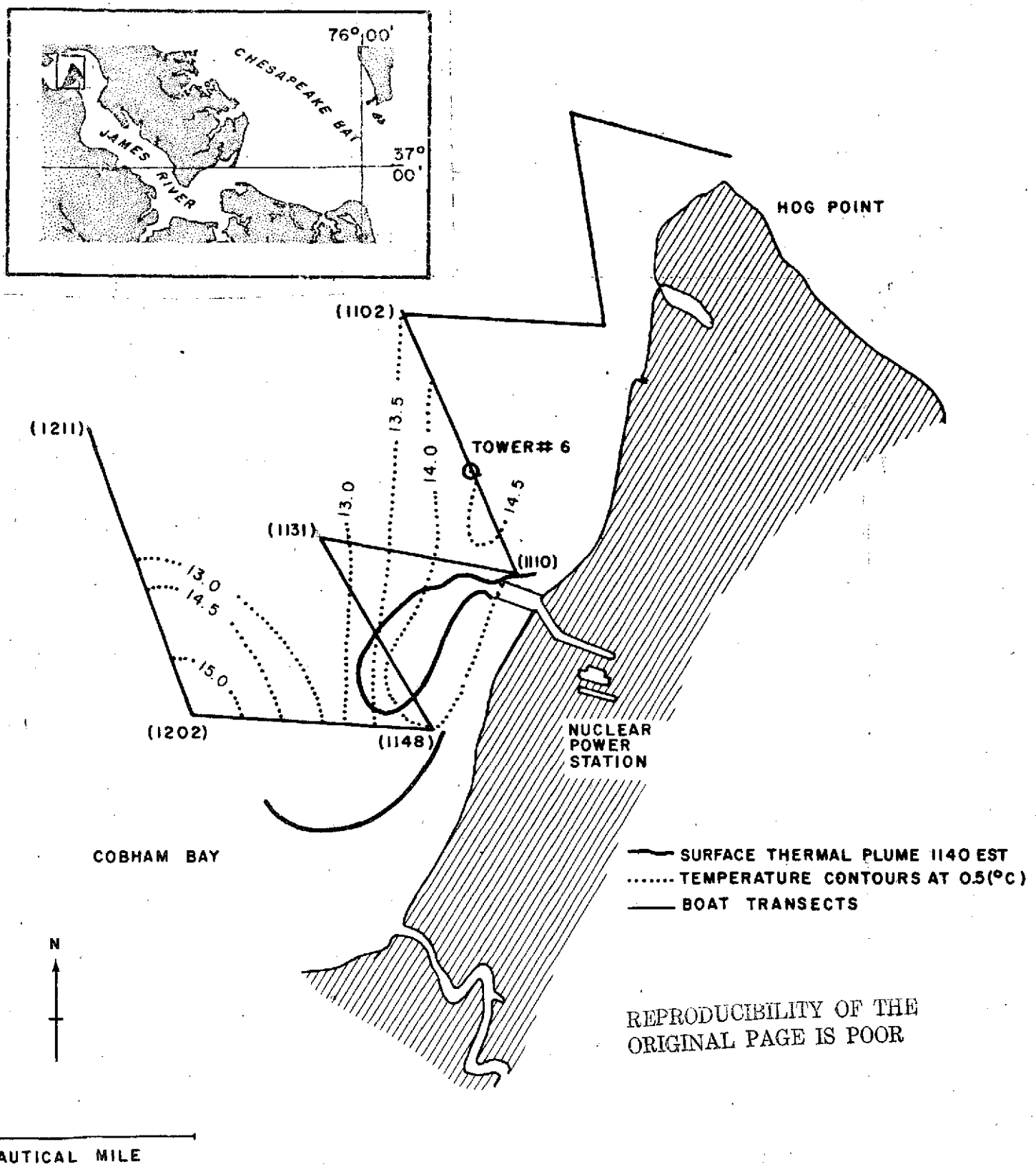

Figure 18. Rectified map showing scanner derived thermal surface plume (1140 EST), boat transects with times (EST), and boat derived isotherms at 0.5 foot depth.

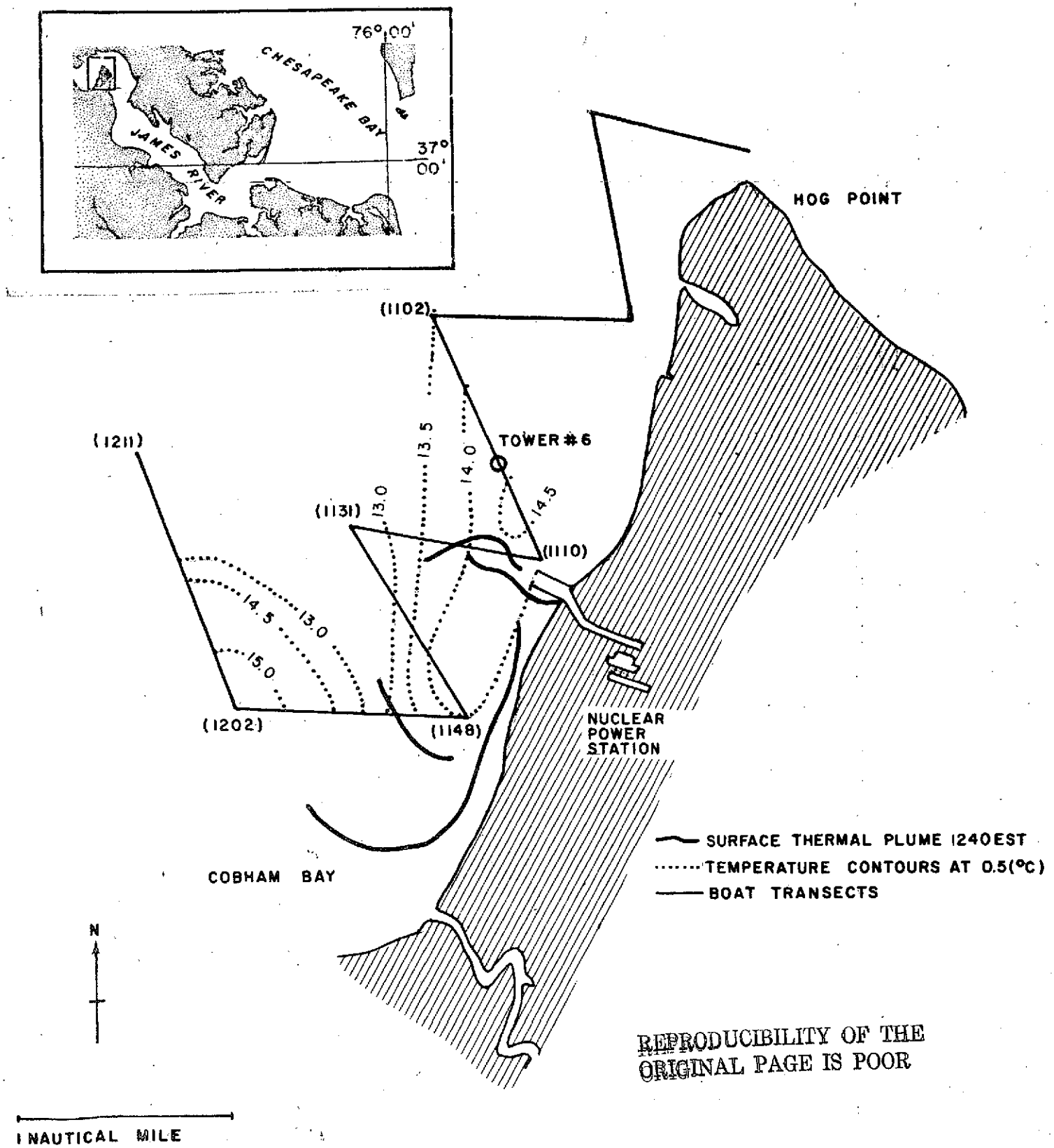

Figure 19. Rectified map showing scanner derived thermal surface plume (1240 EST), boat transects with times (EST), and boat derived isotherms at 0.5 foot depth.

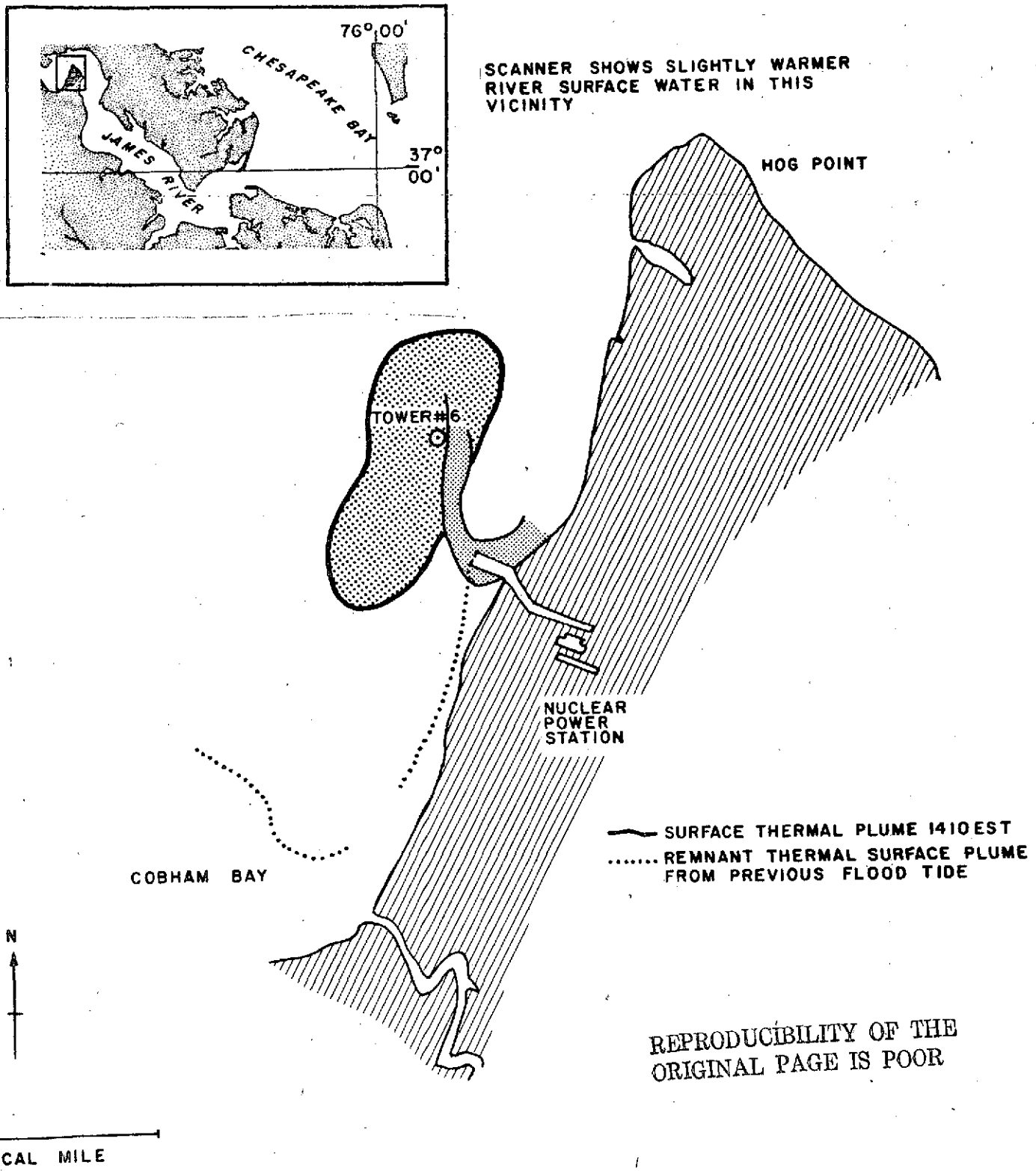

Figure 20. Rectified map showing scanner derived thermal surface plume (1410 EST).

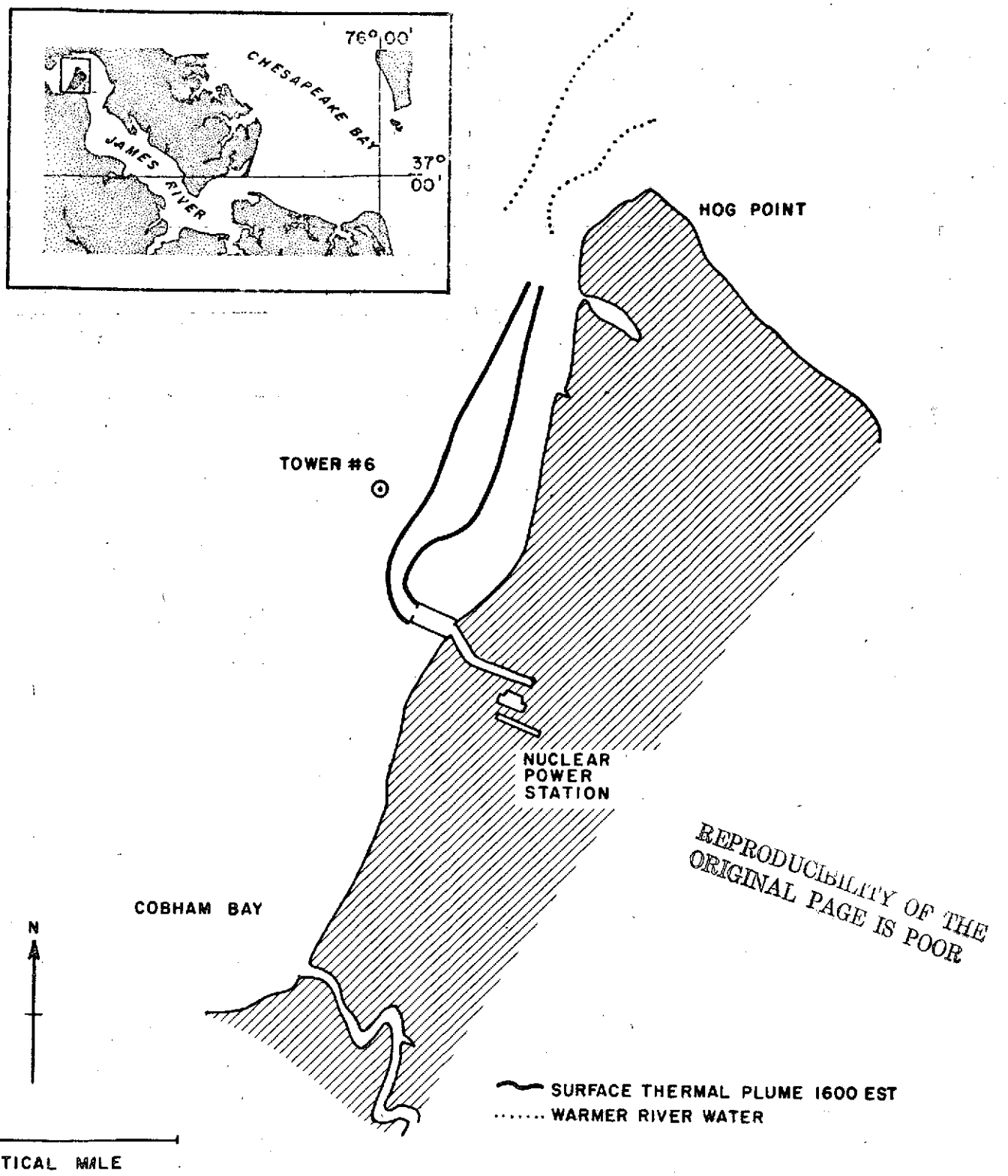

Figure 21. Rectified map showing scanner derived thermal surface plume (1600 EST).

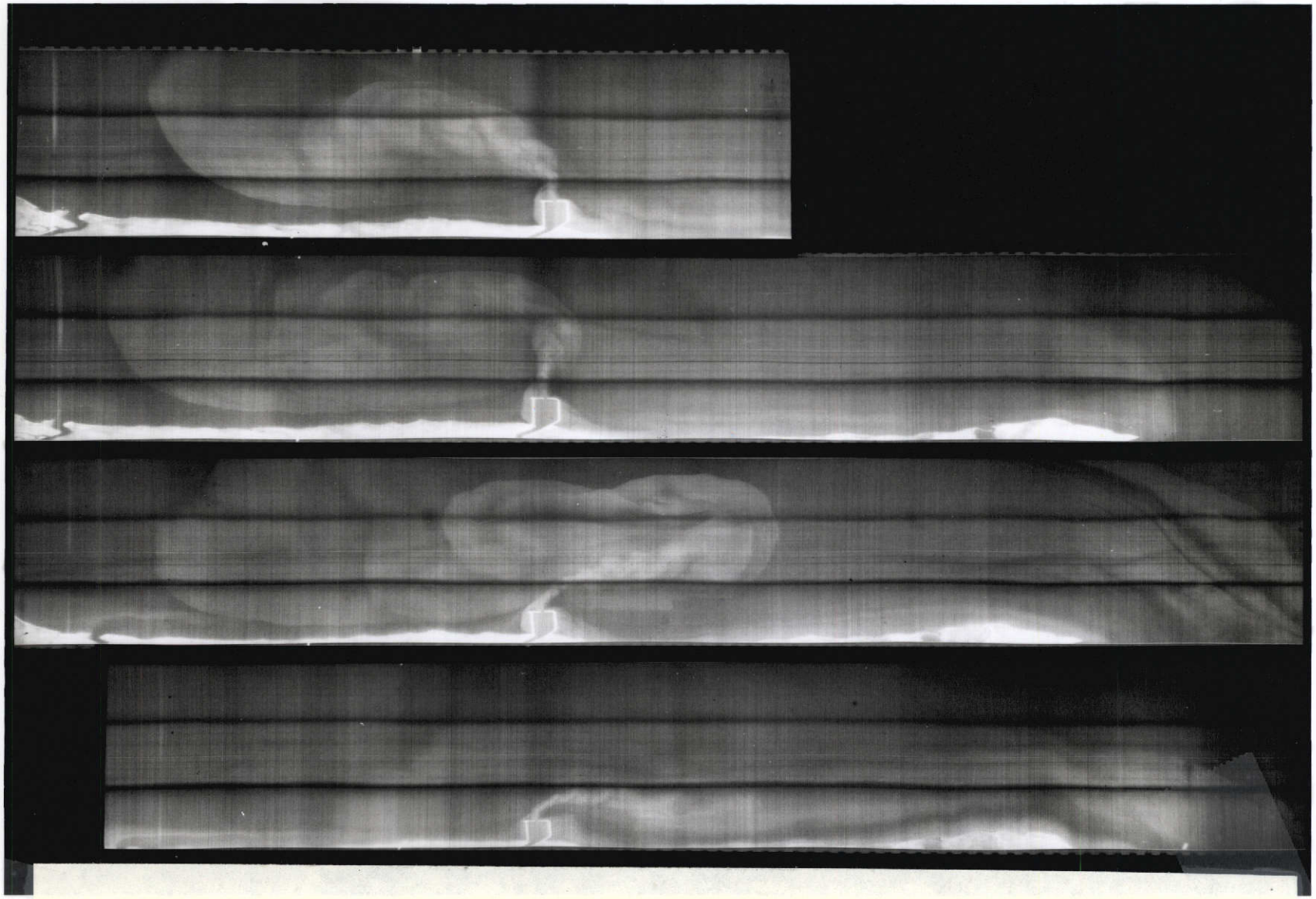

Figure 22. Composite made from four original 70 mm infrared scanner strips (8-14 μm). Times from top to bottom - 1140, 1240, 1410, 1600 EST. Warmer objects appear lighter. Altitude was 2,000 feet over outfall jetty.

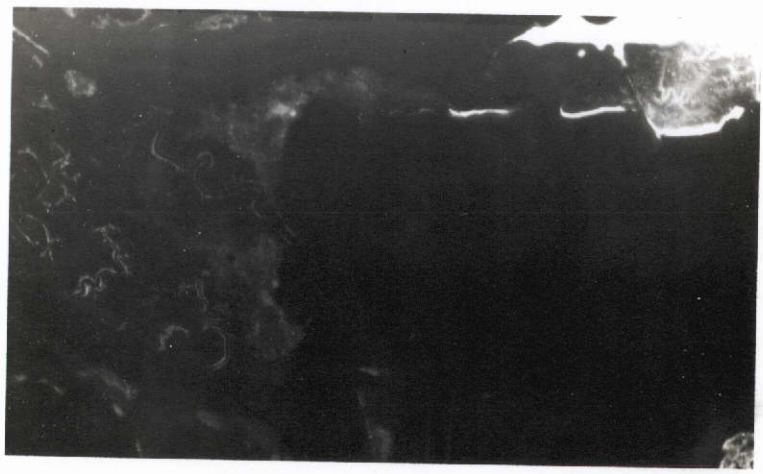

runs were finished. Figure 23 is an unsmoothed plot of temperature at the tower throughout the day at the 0.5 foot depth. Finally Figure 24 is presented to show the discrete areas of differing surface temperature as recorded by the IR scanner. Shown are four black and white reproductions of four color encoded, density sliced portrayals of the scanner strips in Figure 22 (note only a small portion was used). Temperature of the surface layer of water increases from region A to B to C. Variations or banding within each region is caused by shades of the original three colors (blue, violet, brown) which further subdivide the major regions into subregions. For purposes of discussion in this report only the major regions (A, B, C) will be used. The shoreline and discharge jetty have been encoded black for orientation only.

Table III

Conditions at Hog Point on April 17, 1974

Tide (predicted)

Slack	Max Flood	High Water	Slack	Max Ebb	Low Water
0803	1017	1111	1301	1634	1726

Wind

0-5 knots SW at 1200

Nuclear Plant Operational Parameters[1]

Intake Temperature[2]	57.8°F(14.3°C)
Discharge Temperature	66.4°F(19.1°C)

Operation	Unit 1	Unit 2
	86.8%[3]	43.2%

[1] From VEPCO records

[2] At 1200 EST

[3] Based on a 100% output of 788 megawatts and 11.9×10^9 BTU/hr

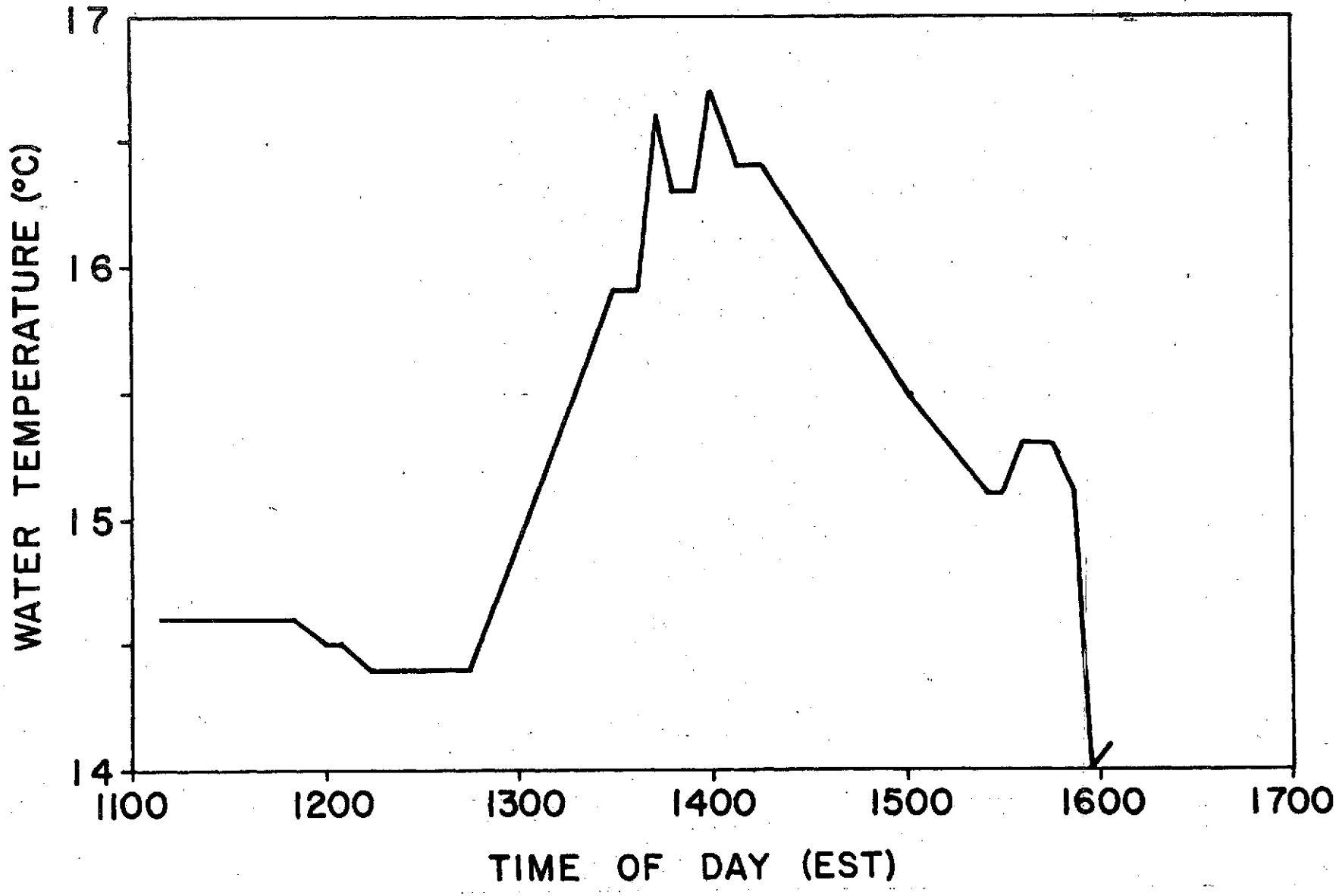

Figure 23. Unsmoothed plot of temperature at tower # 6 vs. time taken 0.5 feet below surface.

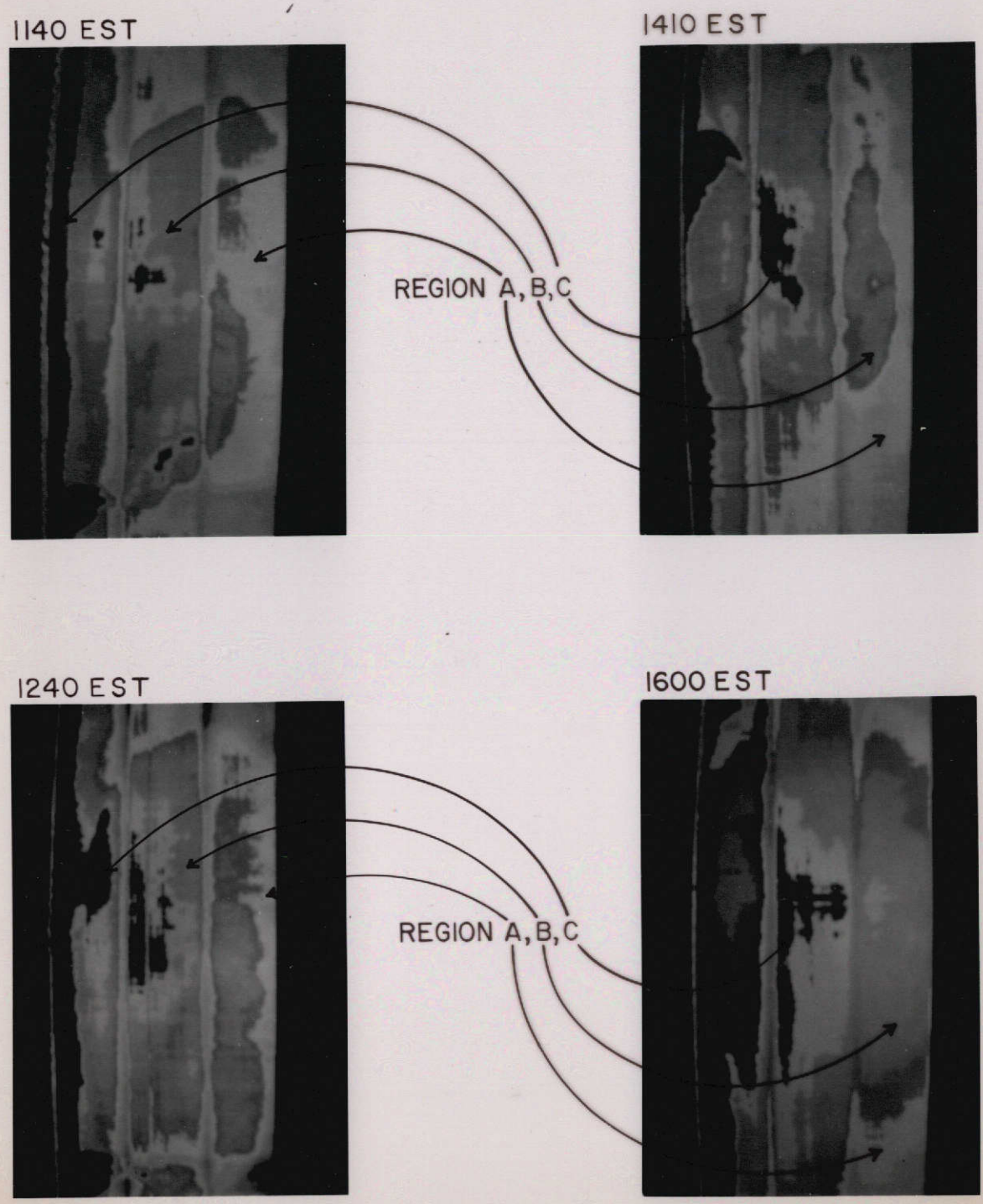

Figure 24. Black and white print of color encoded representations of original scanner imagery shown in Figure 22 (only a portion was used, and scale is not the same as Figure 22, or original). Radiometric temperature increases from blue to violet to brown and from darker to lighter shades (A to B to C).

VIMS Annual Report 1973

p. 44 7th line from bottom typo "reproductio" should be "reproduction"

By analyzing these figures and material in Appendix B the following conclusions were drawn. The temperature at the tower as recorded by the stationary boat and the temperature recorded by the moving boat at the time of its closest approach to the tower agree to within 0.1°C The overall shape of the plume as recorded by the thermal scanner agrees very well with the tide stage in Table III. Figure 22 shows the surface plume at 1240, very near the time of predicted slack water, to be flowing straight from the exit canal jetty with slight curvature in the direction of ebb flow (down river toward Hog Point). In the morning (1140) the surface plume was moving into Cobham Bay and forming a well defined envelope extending approximately 1.5 miles to the north of the outfall. The presence of isolated warm spots within the plume is evident in Figure 24. Figure 18 (the rectified map with boat transects taken at 1140) shows a degree of correlation between the inner warm plume and the 14.0°C contour at the 0.5 foot depth. Care should be exercised in interpreting the rectified maps with boat derived temperature contours since these are drawn using data taken at different locations separated by up to one hour in time. By the 1408 pass, the rectified map (Figure 20), the scanner reporduction (Figure 22), and the color encoded representation (Figure 24) all show a warm "finger" of surface water beginning to move toward the point (downriver), surrounded by a new well-defined surface plume envelope approximately 0.5 by 1 mile. Remnants of the earlier envelope can still be seen in Cobham Bay in Figures 22 and 24. There is good correlation between the warm part of the plume (which is very close to the tower location) and the 2°C rise in water temperature recorded by the stationary boat between

1330 and 1400. When the 1410 pass was made the warm "finger" had apparently just left the tower as evidenced by its location in Figure 20 and the corresponding drop in water temperature at the 0.5 foot level. By 1600, near the time of maximum ebb flow, the scanner shows the plume to be moving from the jetty, folding close to shore, and merging with other warmer water from upriver rounding Hog Point (refer to Figures 21, 22, and 24). The sharp bend made by the plume leaving the jetty indicates a water current which would preclude the formation of a well-defined surface plume as noted earlier.

An attempt was made to correlate the color encoded surface plumes in Figure 24 with temperature measured at the 0.5 foot depth. To test the validity of the correlation we hypothesize it is possible and examine our data for supporting facts. The following assumptions are made: the density of the IR film image varies linearly with surface temperature for equal emissivity targets (over a small temperature range), the color encoding process assigns colors and shades of colors to equal density ranges, and the increase in path length for images at the edge of the scanner field of view does not cause a significant energy loss at 2,000 feet altitude. By the hypothesis the brown shades (C) in Figure 24 will be assigned the range of their highest and lowest measured temperatures, 16.5°C to 19.0°C. 16.5°C was measured at the tower at 1400 when the warmest part of the plume surrounded the tower; 18.6° was measured by the boat at 1615 in the immediate vicinity of the jetty while VEPCO lists a temperature of 19.1°C at noon within the jetty. Using the assumptions, all shades of violet (B) will represent a 2.5°C range as

will all shades of blue (A). The temperature ranges assigned to the colors would then be 11.5 - 13.9°C for blue, 14.0 - 16.4°C for violet, and 16.5 - 19°C for brown. Referring to Figure 18 and the color encoded representation (Figure 24) the instrumented boat passed through the area of the plume coded violet at the time the scanner was making the 1140 overpass. Temperatures recorded by the boat at 0.5 foot depth are in the range of 13-14°C which would be coded blue using the hypothesis. Shortly thereafter the boat passed out of the plume, coded violet, and into the area coded blue in Figure 24. However, toward the end of transect #7 and beginning of #8 there are temperatures at the 0.5 foot depth in the 14-15°C range which would be coded violet using the hypothesis.

The total temperature range at the tower was 2.5°C while that recorded by the moving boat was 3°C. Taken together this represents a range of 4.5°C, whereas the scanner responded to a hypothetical 7.5°C temperature spread. The above facts indicate that the surface thermal plume will not always have a temperature the same as that 0.5 feet below the surface. Indeed, boat data from depths of 0.5 and 3 feet indicate that the surface layer of water may be several degrees warmer than the subsurface in some locations and the same in other places. The original hypothesis is not valid. We are able to define the extent of the surface plume and to delineate the warmer and cooler areas, as well as the maximum plume temperature of 18-19°C. Temperature contours derived from the infrared scanner data are not possible, however, without additional ground truth or scanner calibration.

Continuing Studies

The concentration of work for 1974 will be on correlating infrared imagery and ground data with the power plant in operation. Overflights will be scheduled during periods of extreme and typical plume tidal excursion, and during times of the year when fresh water discharge is maximum or minimum. We suggest, from past experience, planning extra overflights in order to account for weather problems, equipment failure, or other events which might arise. One flight per month, beginning in March when the instrumented boat again resumes its schedule of bi-weekly data runs, should be sufficient.

Coincident with the thermal flights the experiment to find a suitable target easily recognized on the thermal imagery will contunue using a pan of hot charcoal anchored in a special floating platform. It is hoped the temperature of the charcoal will offset its limited area enough to produce a white spot on the film positive.

One additional flightline, parallel to the existing north-south line and slightly farther offshore, should be added to image the tower toward the frame edge to determine how much energy is lost due to the increase in atmospheric path length. This would also allow more reliable placement of the outer edge of the plume and give a better level for the background surface water temperature near the river channel.

A major part of the effort this year will be to examine the surface temperature of the water in relation to the temperature at the 0.5 foot depth to determine the extent to which the plume, as imaged by the scanner, is a surface layer of warmer water over cooler subsurface water. Use of the floating thermistor employed in the

oil experiments conducted by VIMS and NASA Wallops (Gordon and Penney, 1971 and 1972) as well as a radiation thermometer in the aircraft to better assign temperature to scanner film density is suggested.

Finally, a further improvement over last year's techniques will be automation of the geometric rectification-density enhancement process using the NASA Wallops scanning microdensitometer and computer facilities as described previously in this report.

DETERMINATION OF TIDAL VOLUMES IN BARRIER ISLAND SYSTEMS BY SEQUENTIAL BLACK AND WHITE IR IMAGERY

I Introduction

Much of the Atlantic and Gulf coasts are characterized by barrier island complexes comprised of marsh-lagoon systems subject to tidal flushing by inlets. These coastal areas are experiencing increasing pressures of development by man and as a result the water quality of these ecosystems is frequently degraded. Enlightened management of these resources demands a rather complete understanding of the flushing characteristics of the basin and interchange of water via the inlet. The stability of the inlets themselves is central to flushing of the interior basins since empirical evidence (O'Brien, 1969) indicates that the cross-sectional area of the inlet channel controls the tidal prism gated by the inlet. The inlet channel area, moreover, is controlled by the magnitude of littoral drift (tending to choke the inlet) and the hydraulic currents generated by the difference of water levels due to tide fluctuations tending to open the inlet. Thus the inlets can be viewed as the keystone of the flushing of the barrier island system as well as access points to the interior by boats.

The dynamics of inlets are very incompletely understood. It is not possible, for example, to predict specifically how an inlet will change under given conditions of littoral drift tending to close the channel. Recent research on inlet dynamics, however, tends to confirm the fact that the volume of water gated by the inlet to the

interior controls the overall stability of the channel. Furthermore the storage characteristics of the basins (volume stored as a function of water level) determines the distortion of the discharge-time relationship at the inlet channel which thereby determines whether or not sand will be advected into the interior of the inlet channel (Mota Oliveira, 1970).

The Problem. The determination of tidal volumes for various tidal stages in the basins behind barrier island systems is essential to:

1) understanding the behavior of and the design of tidal inlets

2) the determination of flushing characteristics between basins with multiple connections to inlets

Consideration of the typical barrier island system indicates the systems are comprised of channels, subtidal shallows, tidal flats exposed at low tides, and marshes of varying elevation. As the tide rises from low to high stages these morphological elements are sequentially flooded. If there is appreciable marsh area the tidal volume increases very rapidly once the marshes become flooded.

Existing topographic maps and hydrographic maps do not have the necessary vertical resolution to obtain accurate estimates of the tidal volume as a function of tide elevation. To obtain adequate coverage using hydrographic and land surveying techniques of the tidal flats and marshes would be very expensive and time consuming.

II The Approach

The approach used here was to use the water surface itself as a contouring machine as the water surface rises over the variable

topography with rising tide. This was achieved using sequential aerial photo coverage utilizing black and white infrared film which enhances the contrast between flooded and exposed surfaces. In order to determine the vertical changes in tidal elevations during the sequential flights tide gages were installed within the study area. The volume storage as a function of tide stage could then be computed as the product of incremental increase in the surface area flooded and the corresponding incremental rise in tide elevation. The details of the procedure are discussed later.

The experimental test site chosen was that segment of the barrier island marsh lagoon complex on the Eastern Shore of Virginia which is flooded by the prism gated by Wachapreague Inlet. This study area is shown in Figure 25. The rational for this choice was that a substantial understanding of the hydraulics of that system had been achieved (Byrne, et al., 1973). This background information included direct measurements of the prism gated by Wachapreague Inlet and an estimated storage relationship based on observation of the tidal stages which appeared to initiate flooding of the bays and marshes and a determination of the relative area of marshes, bays and channels. The rather poor correlation between measured prisms by integration of instantaneous discharge at the inlet and those calculated from the estimated storage function led to the decision to attempt the method herein discussed.

The goal of the study, then, was to obtain a storage curve which relates the volume of water within the system serviced by Wachapreague Inlet to the tidal stage at Wachapreague Dock tide gage. The tidal prism for any given tide can then be obtained by subtraction of the

Figure 25. Study area; storage basin for Wachapreague Inlet.

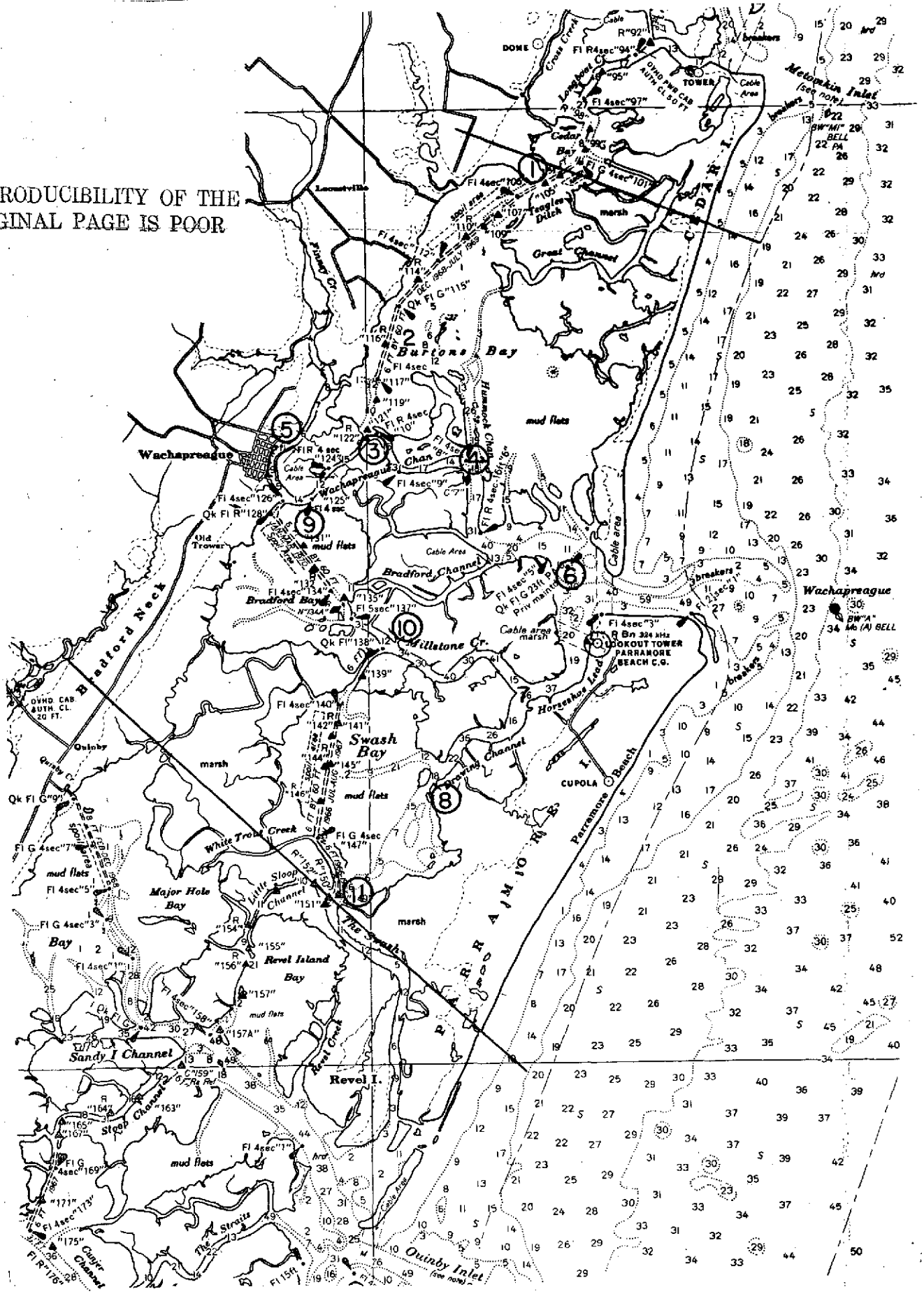

low water volume from the high water volume. This capability is important to the detailed understanding of inlet response because two tides of the same range but differing maximum stage will have different prisms and therefore different scouring capacities at the inlet channel.

III Methods

A. Mission Plan. The mission plan was to image the flooded surface of the study area at 30 minute intervals as the tide level rose from low to high water. During the overflights tidal elevations were monitored at eleven sites within the system, and tidal discharges were measured at the two interior channels, The Swash and Teagles Ditch, which connect the Wachapreague marsh lagoon system with the adjacent systems serviced by the adjacent ocean inlets.

Mission W226, Flight 1, was accomplished on 28 June, 1973, utilizing the Wallops Station C54 aircraft equipped with two T-11 aerial mapping cameras using 152 mm lenses. The film was type 2424 black and white infra-red with a clear anti-vignetting and 89B filter combination. The flight was made in hazy weather with broken clouds. Visibility was from 5-7 miles. Nominal flight altitude was 9,500 feet with a wind of 19 knots from 220°.

Twelve groups of three lines each were flown at approximately thirty minute intervals from 1300 to 1900 EDST. The orientation of the lines made the photography generally suitable for mosaicing; however, four of the twelve groups could not be used due to one or more of a combination of excessive tip and tilt, crabbing or lack of

sufficient overlap. The complete mission summary is available from NASA Wallops Station, Chesapeake Bay Ecological Program Office.

The flight date was chosen so that the existing conditions represented a rising spring tide during daylight hours. A rising condition was specifically chosen so that initially drained tidal flat faces would be as "dry" as possible.

B. Analysis of Data.

1) Ground measurements. The positions of the tide elevation measuring stations are shown in Figure 25 and listed in Table 4. Stations 5 and 6 are long-term recording tide gages for which tidal elevation data planes have been determined. The remainder were temporary tide staffs installed on the mission date. Inspection of Table 4 indicates a phase lag of up to 0.7 hr. and a range difference of up to 0.4 ft. across the system. The most extreme comparison, that between Wachapreague Inlet and Wachapreague Dock, is shown in Figure 26 referred to long-term mean tide level which is assumed to be a level surface. Inspection indicates a water slope of 0.5 - 0.6 ft. exists between the two positions during the central portion of the rising phase. This fact that the water surfaces slope during the tide cycle necessitates the introduction of a correction factor since the tide gage at Wachapreague Dock will underestimate the volume of water in the system on the rising tide. Long-term comparisons between these two gages show an average range difference of 0.2 ft. and 0.6 hr. phase lag.

Discharge measurements at The Swash (#11 in Figure 25) and Teagles Ditch (#1 in Figure 25) indicated that tidal water enters

TABLE 4

Tide Elevation Data for 28 June, 1973

Station	Tide Range (ft.)	Time Low Water	Time High Water
1	----	----	18.5
2	5.4	11.8 hr	18.4
3	5.5	11.8	18.5
4	5.4	11.3	18.2
5	5.7	12.0	18.7
6	5.3	11.3	18.3
7	----	11.4	18.2
8	5.6	11.6	18.5
9	5.7	11.7	----
10	5.6	11.0	18.3
11	5.6	12.0	18.5

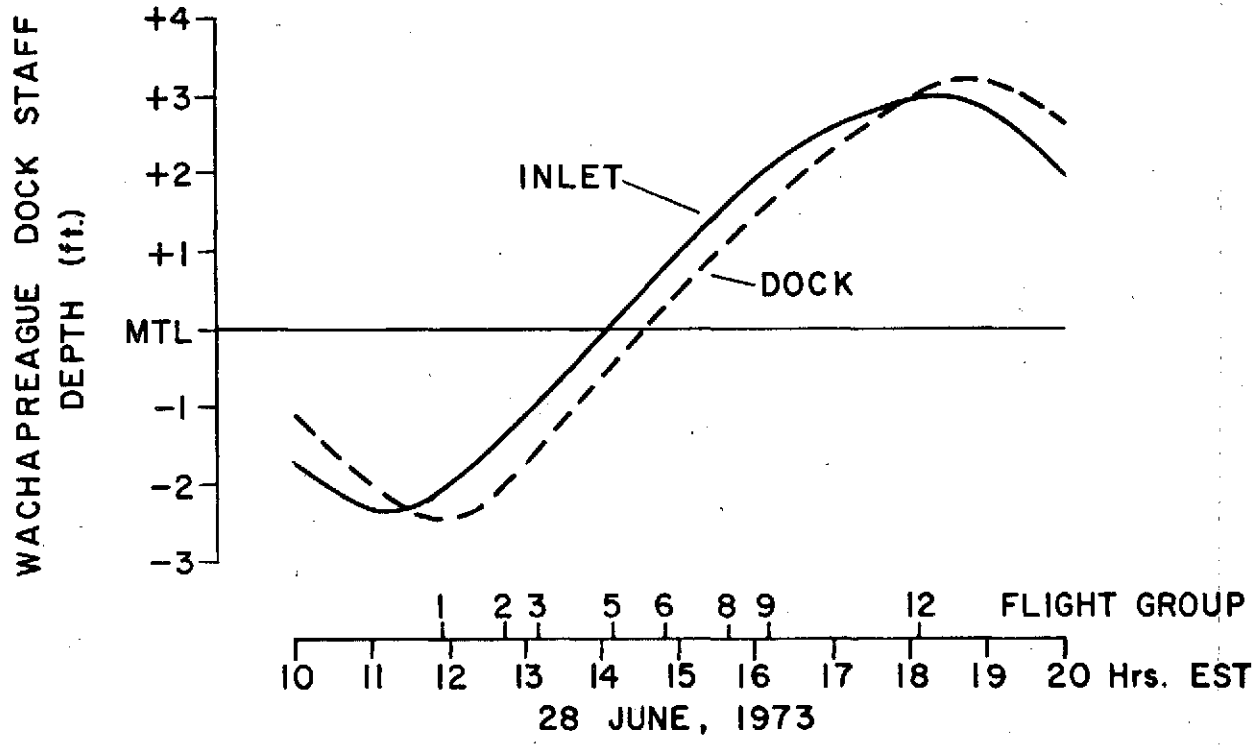

Figure 26. Tidal elevation curves for Wachapreague Dock and Inlet during Mission W 226, Flt. 1.

the Wachapreague Inlet Basin system during the first part of rising tide and exits during the latter part. Measurements on 28 June 1973 give:

Swash	Teagles Ditch
Into system 69,000 m^3	Into system 400,000 m^3
Out of system 99,700 m^3	Out of system 548,000 m^3

This will be shown to be a negligible fraction of the total volume held in the system. Thus, the effects of this "leakage" are ignored hereafter.

2. Imagery Analysis. Reproductions of the original transparencies were used in the analysis. Eight of the twelve flight groups were assembled into mosaics of the 28.9 square nautical mile ($86.65 \times 10^6 m^2$) area.

The major absolute errors in the mosaicing procedure occur in aligning some sixteen frames having various edge distortions and in determining and cutting conjugate boundaries properly. These errors are indeterminate and are presumed random.

Determinations of the non-water covered areas in each mosaic were determined using the I^2S Digicol located at NASA-Langley. Water areas were determined by subtraction from total area. The instrument was adjusted so that exposed surface area could be coded as one color while the water covered surfaces and the masked areas registered an off-scale black. Absolute area calibrations were accomplished using masks of known area and plotting these areas versus Digicol-indicated percentage area. All mosaics were analyzed on the same day, a considerable saving in time over hand planimetry.

In order to specify film density boundaries associated with water boundaries, the water boundaries were visually identified with a sharp tipped pointer and the instrument settings were then adjusted to shift the boundaries to the proper position. This procedure was clear cut at tide levels below the marsh surface. At higher levels, marsh plants significantly decreased boundary contrast but sun glint assisted in boundary interpretation. For several runs analyzed more than once on different days total water areas varied as much as 5 percent which revealed a day to day bias in interpretation. These problems would likely be reduced if initial film exposure could be adjusted to give high contrast for very shallow depths. The exposures during the mission were adjusted to give maximum definition of water color differences and not maximum contrast between flooded and non-flooded surface. Contrast was heightened in reproduction of the transparencies. An example of the imagery is shown in Figure 27a, b for a conjugate area at a)low and b) high tide elevations.

IV Results: Analysis for flooded area and storage volume.

The times of the flight groups used in the analysis, relative to tidal stage are shown in Figure 26. Using flight times and the water area determined from the sequential mosaics the relationship between flooded area and stage at the Wachapreague Dock was constructed as shown in Figure 28. Observed area changes extended over the range in stage from 1.8 ft. to 7.2 ft. at the Dock gage. Since the water surface slopes up to as much as 0.6 ft. between the Wachapreague Dock and Inlet gages the flooded area measured is not the same as would be indicated if the surface was level across the area.

Figure 27. Examples of imagery for conjugate areas; a) Flight Group 1 and b) Flight Group 12 (time key relative to tidal heights is given in Figure 26).

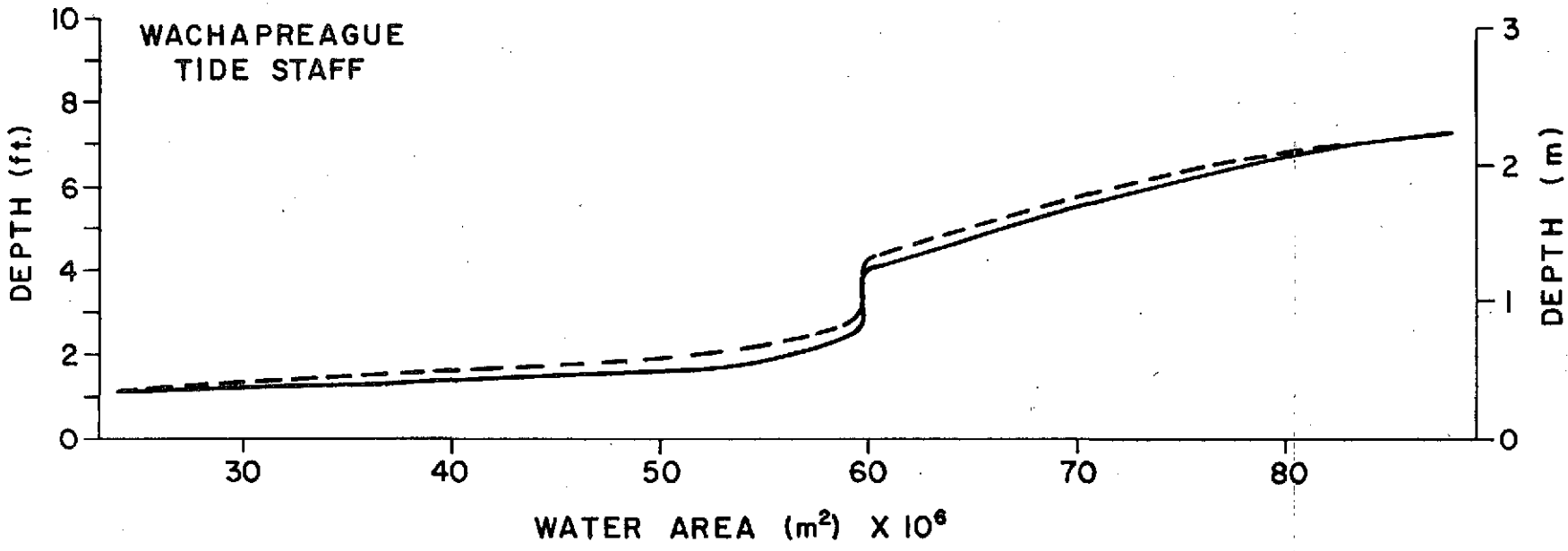

Figure 28. Area of flooded survace as a function of tidal stage at Wachapreague Dock. Solid line is raw data, dashed line is rectified to account for water slope.

In order to make a first order correction it was assumed that at any particular tide stage the surface area flooded is equal to that at the stage $\frac{1}{2}\Delta Z$ (Figure 26) lower. This shifts the curve to lower flooded area for a particular stage (dotted line, Figure 28). The segment of the curve between stages 2.5 and 4.3 ft. indicates constant flooded area. This represents the near vertical banks of much of the major embayment, and that area, $59.5 \times 10^6 m^2$, represents the cut-off between areas of channels, flats, and bays and areas of marshes. This and other ancillary information are useful in extending the curve of flooded area versus stage to stages lower than the 1.8 ft. observed. Visual observations and scattered measurements on the ground indicated about 0.5 ft. water depth in the bays at 1130 hrs. on the 28 June. Thus, the cut-off for initiation of flooding in the bays was taken at 1.3 ft. on the Dock gage. Previous work (Byrne et al., 1973) utilized an estimated storage function based upon the areas of channels, marshes and bays and the artificial assumption that the bottom elevations of the bays and the marshes were uniform. The measured areas were:

Channel (major only)	$8.087 \times 10^6 m^2$
Bays	$34.8 \times 10^6 m^2$
Marsh (including drainage channels)	$49.304 \times 10^6 m^2$

The cut-off elevations were taken as 2.5 ft. and 5.5 ft. respectively for bays and marshes. The curve in Figure 28 indicates that the total channel area, including the drainage channel in the marsh, and the bays totals to $59.5 \times 10^6 m^2$. It is reasonable to assume that the area of bays is correct at $34.8 \times 10^6 m^2$. Thus this total channel area must be about $24 \times 10^6 m^2$. This allows a statement of the component

areas within the imaged area as:

Channels	$24.0 \times 10^6 m^2$
Bays	$34.8 \times 10^6 m^2$
Marsh	$37.6 \times 10^6 m^2$

Given the above, the curve in Figure 29 may be extended to the channel cut-off; $24 \times 10^6 m^2$ at 1.3 ft. on the Dock gage.

The cumulative volume of water stored in the marsh-bay-channel system was computed from the curve in Figure 28 using incremental volumes for every 0.5 ft. stage increase at the Dock gage. The volumes are referred to 0 elevation of that gage which insures inclusion of all observed tides within the last three years. The assumption was made in the calculations that the flooding for each incremental increase in stage occurred over a uniformly sloping bottom. The cumulative volume versus gage is shown in Figure 29. The figure also shows the originally estimated volume using channel, bays and marshes as components with discreet cut-off elevations. The curve has been extended from the 7.2 ft. to the 10 ft. stage since visual observation indicated the entire system was flooded at stages beyond 7.2 ft. The shift to the left of the storage curve based on the imagery relative to that originally estimated is due to adoption of the 1.3 ft. stage as the cut-off between channel flooding and the initiation of bay flooding.

The storage relationships shown in Figure 29 are compared with tidal volumes measured at Wachapreague Inlet in Table 5. The observed values were determined by integration of instantaneous tidal discharge measured by current meter arrays at the inlet throat. Although accuracy of the directly measured prisms is not known, the measurements

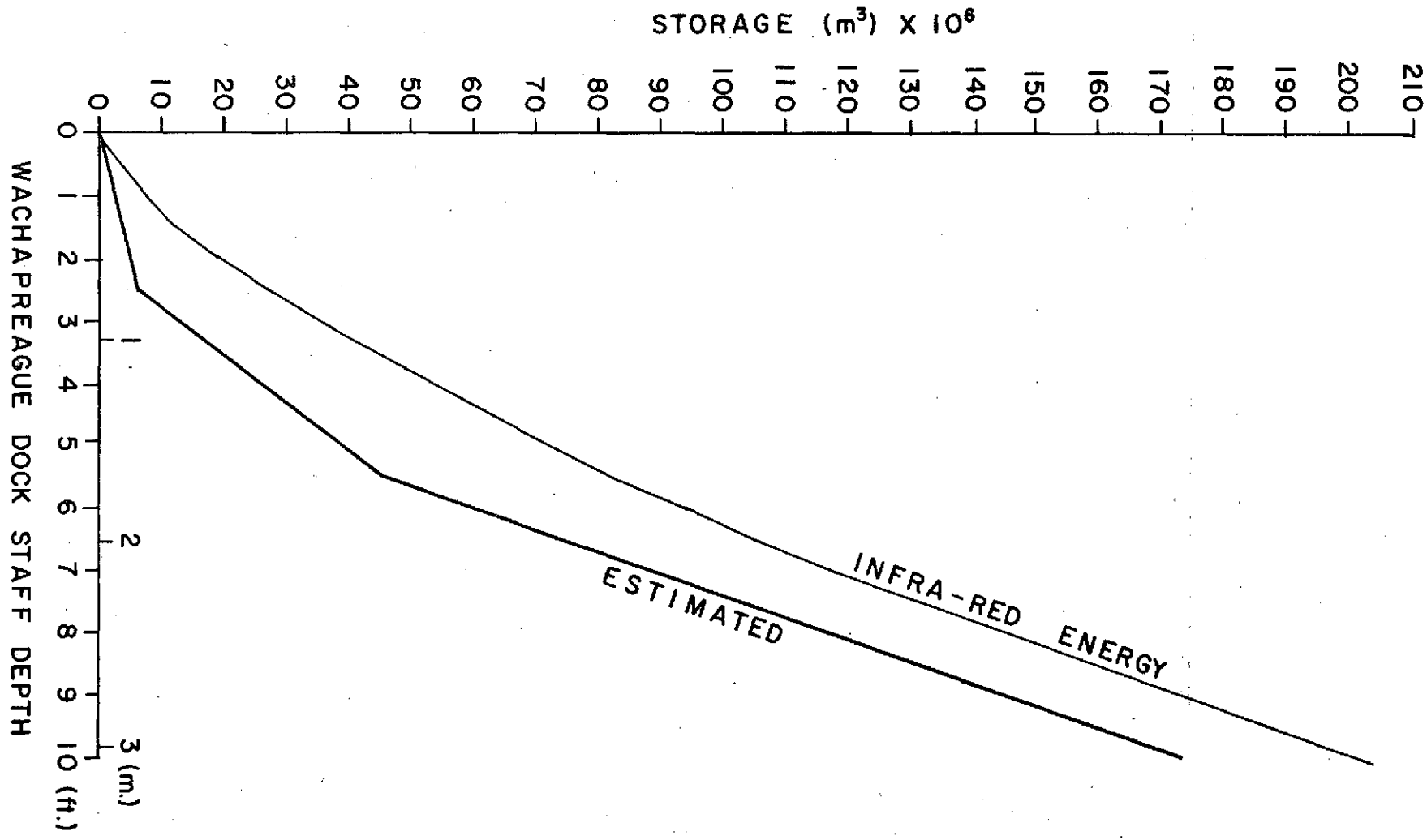

Figure 29. Storage function for Wachapreague Inlet basin as determined by infra-red imagery and as originally estimated.

TABLE 5

Comparison of measured tidal volumes at Wachapreague Inlet with volumes indicated by imagery and estimated storage.

Tide Cycle Number	Date	Tide stage at high and low m (ft.)	TIDAL PRISM (m^3) P_o measured at inlet	P_1 from imagery	P_2 from estimated	% Diff $\left(\frac{P_{1,2}-P_o}{P_o}\right)$ P_1	P_2
1	14 July 70	2.01(6.6)-.79(2.6)	64.9×10^6	78×10^6	67.9×10^6	+20.2	+ 4.7
2	14 July 70	2.01(6.6)-.85(2.8)	62.2	74.5	65.3	+19.8	+ 5.0
3	25 Aug. 71	1.86(6.1)-.79(2.6)	57.4	66 66	53.9	+15.0	- 6.2
4	13 Sept. 72	1.95(6.4)-.98(3.2)	63.2	63	54.4	- 0.3	-13.9
5	13 Sept. 72	1.73(5.7)-.98(3.2)	47.6	47.5	34. 7	- 0.2	-27.0
6	14 Sept. 72	1.73(5.7)-.94(3.1)	45.5	49	36	+ 7.7	-20.8
7	14 Sept. 72	1.86(6.1)-.94(3.1)	61.0	58	47.3	- 4.9	-22.5

represent the best available estimates. Comparison of cycles 3 and 7 in Table 5 indicates an inconsistency in the measured values; both cycles had the same maximum stage but the minimum stage of cycle 3 was 0.15 m less than cycle 7. In actuality cycle 3 must have had a larger prism than cycle 7 but the measurements indicate the converse. A similar inconsistency exists between cycles 5 and 6 although to a lesser degree. The data for measured prisms indicated the accuracy is no better than ±10%.

Inspection of the percent differences between measured prism and that deduced from the imagery and the original estimated storage indicates that volumes deduced from the imagery are in appreciably better agreement with the measured than are those from the estimated storage. The average absolute differences are 9.7% and 14.3% respectively. As previously mentioned the "leakage" from the Wachapreague storage system via the interior channels, The Swash and Teagles Ditch, does not appear to significantly influence the error in estimating the storage from the imagery; the prism for the tide cycle used to construct the storage curve was 106.5 x $10^6 m^3$, while data listed in earlier paragraphs for the volume passage in The Swash and Teagles Ditch combined amount to less than 1% of that figure. Thus, it appears justified to disregard this contribution to the storage.

V Discussion

The present study demonstrates the feasibility of utilizing sequential black and white infra-red photography to determine the storage characteristics of complex basins wherein the flooded area changes irregularly with varying stages of rising and falling tides.

This procedure resolves the problems encountered with determination of tidal prism based on estimates of basin area at high and low water due to the ambiguity of these determinations in shallow irregular basins (O'Brien, 1969; O'Brien and Clark, 1973). The method offers great potential value in tidal inlet studies as it offers the opportunity to specify the expected average discharge for any particular tidal condition. Furthermore, if the inlet channel cross-sectional area is known, the average ebb and flood currents for any given tidal cycle may be derived. This information may be then summed over a longer period (months, seasons, years) for which reference tide records exist to estimate whether the inlet currents advect sand into or out of the inlet (Byrne et al., 1973).

The methodology also offers very interesting possibilities as an alternate approach to constructing depth contour maps. The primary mission of the National Ocean Survey's hydorgraphic mapping activities is to provide highly reliable maps for navigation purposes. Typically, in areas where such studies are done the channels are carefully delineated but less emphasis is given to the shallow bays and no attention is given to the variable marsh elevation. State of the art numerical models for flushing such as the Jamaica Bay Study (Leendertse et al., 1973) require moving boundary conditions which necessitates fairly high resolution depth maps. Such maps could be constructed using the described technique wherein the instantaneous waterline acts as a contour. This approach would be quite successful in those areas where there is not appreciable tide range variation within the basin system; such as the Wachapreague System.

Finally, it should be noted that the technique offers a possible method to study tidal range variations in those basins with large range and phase differences within the system. Existing methods involve the installation of a large number of tide gages and a data base over a period of one month or longer. The tidal datum plane is then established and mean range and phase differences determined. In those areas where such detailed surveys cannot be conducted the method discussed herein would supply very useful data. It is also likely that application of the method would be useful in planning tide gage locations for a detailed survey. In such applications the stage variations as a function of time would be measured using stereophotogrammetric techniques.

Acknowledgments

This study was supported, in part, by Office of Naval Research, Geography Programs, Contract No. NOOO 14-71-C-0334, Task 388-103. We wish to thank J.T. DeAlteris, J. Sovich, D.J. Tyler, M. Carron, W. Mohr, E. Hogge and D. Byrd for assistance in the ground measurements. The idea for the approach arose during discussions between the senior author and Dr. John D. Boon, III who has since applied the technique to storage volumes in a small marsh system (Boon, 1973).

A P P E N D I X A

Reflectances

FLIGHT 1 RUN 1

POINT	REFLECTANCES FR 1	FR 2	FR 3	FR 4	FR 5	FR 6	FR 7	FR 8	FR 9	FR10	FR11	FR12	AVG	SIGMA
M2	1.8	1.6	1.4	1.8	2.5	4.1	7.8	****	****	****	****	****	3.0	2.2
M1	****	6.5	6.5	6.1	7.3	5.9	5.7	5.3	6.5	****	****	****	6.2	0.5
15	5.7	4.2	3.8	4.7	3.6	5.9	6.3	****	****	****	****	****	4.9	1.0
33	4.5	3.8	3.2	3.5	4.2	6.5	****	****	****	****	****	****	4.3	1.1
25	8.7	6.3	5.2	5.3	5.2	3.2	4.8	5.7	****	****	****	****	5.6	1.5
11	8.2	6.5	5.3	4.4	4.1	4.1	4.1	4.1	****	****	****	****	5.1	1.5
18	7.3	6.3	5.0	3.6	3.6	3.6	3.5	4.2	****	****	****	****	4.6	1.4
14	15.6	11.3	8.5	7.8	7.3	6.5	6.1	6.5	9.5	****	****	****	8.8	3.0
19	10.4	7.5	5.5	4.4	3.4	2.9	3.0	3.6	6.1	****	****	****	5.2	2.4
28	****	13.6	11.0	6.9	11.6	4.5	5.5	8.0	8.7	****	****	****	8.7	3.1
9	14.8	8.2	11.0	10.7	10.4	9.2	9.2	9.0	11.0	****	****	****	10.4	1.9
22	****	****	12.6	9.8	10.4	7.8	7.8	6.3	6.7	****	****	****	8.7	2.2
24	****	14.8	11.9	10.7	10.1	9.0	8.5	7.3	****	****	****	****	10.3	2.4
10	****	****	16.4	14.0	13.3	9.0	7.3	7.5	9.0	****	****	****	10.9	3.5
26	****	18.7	14.0	17.3	12.9	11.6	9.5	11.0	17.8	****	****	****	14.1	3.4

FLIGHT 1 RUN 2

POINT	REFLECTANCES FR 1	FR 2	FR 3	FR 4	FR 5	FR 6	FR 7	FR 8	FR 9	FR10	FR11	FR12	AVG	SIGMA
M2	3.2	3.0	2.6	3.8	4.4	6.7	9.2	****	****	****	****	****	4.7	2.4
M1	****	6.5	6.1	6.7	6.5	7.1	6.7	6.9	6.9	****	****	****	6.6	0.3
15	6.7	5.0	4.2	4.4	4.2	5.5	7.3	****	****	****	****	****	5.3	1.2
33	4.7	4.4	3.4	4.1	3.9	5.3	****	****	****	****	****	****	4.3	0.6
25	7.8	5.5	3.9	3.8	3.2	3.8	4.5	****	****	****	****	****	4.6	1.5
11	8.2	5.9	3.9	2.9	2.5	3.5	3.1	4.1	****	****	****	****	4.3	1.9
18	6.5	5.5	3.9	3.4	3.2	3.2	3.1	4.2	****	****	****	****	4.1	1.2
14	10.7	8.0	7.1	6.1	5.7	5.5	5.3	5.7	6.3	****	****	****	6.7	1.7
19	****	5.9	4.5	3.1	2.5	2.3	2.4	3.0	3.9	****	****	****	3.5	1.2
28	****	11.9	9.0	8.5	6.9	6.5	9.0	8.7	10.4	****	****	****	8.8	1.7
9	11.3	10.1	7.8	7.3	9.2	8.5	7.8	8.7	8.7	****	****	****	8.8	1.2
22	****	****	9.5	8.7	7.3	7.1	5.2	5.0	7.5	5.9	****	****	7.0	1.6
24	****	10.7	8.7	8.5	7.5	7.1	6.7	5.3	7.1	****	****	****	7.7	1.5
10	****	****	14.8	12.9	9.8	8.7	5.5	6.7	6.9	6.3	****	****	8.9	3.3
26	****	15.2	14.8	12.6	8.0	8.7	8.7	8.5	13.3	****	****	****	11.2	3.0

FLIGHT 1 RUN 3

POINT	REFLECTANCES FR 1	FR 2	FR 3	FR 4	FR 5	FR 6	FR 7	FR 8	FR 9	FR10	FR11	FR12	AVG	SIGMA
M2	3.9	3.5	3.6	3.5	3.6	4.1	5.2	7.8	****	****	****	****	4.4	1.4
M1	****	****	6.5	6.7	7.1	6.5	6.7	6.9	6.7	6.7	****	****	6.7	0.2
15	6.7	6.5	4.8	4.4	3.8	3.9	4.8	6.7	****	****	****	****	5.2	1.2
33	4.8	4.5	3.9	3.9	3.6	4.2	5.7	****	****	****	****	****	4.4	0.7
25	****	11.9	6.1	4.4	3.8	3.8	3.2	3.4	4.5	****	****	****	5.1	2.8
11	****	6.9	5.9	4.7	3.9	2.9	3.0	3.0	3.9	****	****	****	4.3	1.4
18	****	6.5	5.9	4.7	3.5	2.9	3.1	3.4	3.9	****	****	****	4.2	1.3
14	****	****	9.0	6.9	6.7	5.7	5.5	5.2	5.2	5.9	****	****	6.2	1.2
19	****	****	6.9	5.2	3.9	2.4	2.1	2.4	2.6	3.5	****	****	3.6	1.6
28	****	****	11.0	10.7	9.2	7.1	6.3	7.1	8.5	11.0	11.6	****	9.1	1.9
9	****	****	9.8	9.0	7.1	6.9	6.7	6.1	6.7	6.5	****	****	7.3	1.3
22	****	****	****	6.1	5.3	5.7	6.7	7.5	9.0	5.2	6.3	****	6.5	1.2
24	****	****	10.1	10.1	9.2	7.5	7.1	5.3	7.3	6.7	****	****	7.9	1.7
10	****	****	****	****	14.4	11.6	8.7	8.2	7.1	5.7	6.7	****	8.9	3.0
26	****	****	18.2	14.0	14.0	10.7	8.5	9.0	11.3	11.3	11.9	****	12.1	2.9

FLIGHT SUMMARY, FLIGHT 1

POINT	AVG	SIGMA
M2	4.09	2.10
M1	6.56	0.44
15	5.17	1.14
33	4.36	0.82
25	5.17	2.05
11	4.58	1.62
18	4.38	1.29
14	7.32	2.37
19	4.18	1.99
28	8.96	2.26
9	8.95	1.93
22	7.40	1.91
24	8.61	2.19
10	9.61	3.32
26	12.50	3.25

FLIGHT 2 RUN 1

POINT	REFLECTANCES FR 1	FR 2	FR 3	FR 4	FR 5	FR 6	FR 7	FR 8	FR 9	FR10	FR11	FR12	AVG	SIGMA
11	9.5	7.8	7.3	6.6	3.7	4.9	5.5	5.9	****	****	****	****	6.4	1.8
M1	****	5.3	3.2	3.8	3.7	4.2	4.4	4.4	5.3	****	****	****	4.3	0.7
33	3.2	2.1	2.1	8.1	3.2	4.7	****	****	****	****	****	****	3.9	2.2
25	9.5	7.1	6.8	5.7	5.5	5.1	5.1	6.1	****	****	****	****	6.4	1.4
14	****	****	13.6	11.7	9.8	9.2	8.1	9.5	12.1	****	****	****	10.6	1.9
19	****	7.8	7.1	5.3	3.7	2.9	3.2	3.5	5.1	****	****	****	4.8	1.8
M2	16.6	3.5	5.1	4.4	4.2	4.7	5.1	****	****	****	****	****	6.2	4.6
15	2.1	2.1	1.7	1.7	2.5	3.7	4.9	****	****	****	****	****	2.7	1.1
18	8.9	6.4	5.1	4.7	3.2	3.8	3.8	4.5	****	****	****	****	5.1	1.8
26	****	25.5	13.2	14.0	13.6	13.2	12.8	16.6	14.0	****	****	****	15.4	4.2
10	****	****	18.5	12.1	11.1	8.4	6.4	8.6	9.5	7.8	****	****	10.3	3.7
22	****	****	****	16.6	12.1	11.1	9.2	8.9	9.2	9.2	****	****	10.9	2.7
24	****	****	17.0	17.0	12.8	12.8	12.1	12.1	13.6	****	****	****	13.9	2.1
28	****	11.1	8.4	6.1	3.5	5.7	4.2	5.9	7.1	****	****	****	6.5	2.3
9	****	19.0	12.1	14.8	12.8	12.5	11.7	12.8	14.0	****	****	****	13.7	2.3

FLIGHT 2 RUN 2

POINT	REFLECTANCES FR 1	FR 2	FR 3	FR 4	FR 5	FR 6	FR 7	FR 8	FR 9	FR10	FR11	FR12	AVG	SIGMA
11	6.6	5.3	3.3	2.6	2.8	3.0	3.0	2.5	****	****	****	****	3.6	1.4
M1	5.1	4.4	3.5	3.3	3.3	3.0	3.8	3.5	4.9	****	****	****	3.9	0.7
33	1.7	1.8	2.1	3.2	4.2	****	****	****	****	****	****	****	2.6	1.0
25	7.6	5.3	4.0	2.5	3.3	2.3	3.7	3.7	****	****	****	****	4.0	1.6
14	12.5	10.4	8.6	7.3	6.4	4.9	4.5	5.3	7.8	****	****	****	7.5	2.6
19	6.8	5.1	2.9	1.6	1.4	1.0	1.4	1.7	4.4	****	****	****	2.9	2.0
M2	4.2	4.2	4.0	4.0	4.7	4.7	****	****	****	****	****	****	4.3	0.3
15	2.9	2.5	2.0	2.6	3.5	4.2	6.8	****	****	****	****	****	3.5	1.6
18	5.1	3.7	2.2	1.6	1.5	1.7	2.2	2.1	****	****	****	****	2.5	1.2
26	****	17.5	13.6	11.1	12.5	11.1	8.1	9.8	12.8	11.4	****	****	12.0	2.6
10	****	****	11.4	8.6	8.4	5.5	5.1	5.1	4.9	5.3	****	****	6.8	2.3
22	****	****	11.7	10.7	8.9	7.3	5.9	5.9	5.3	5.3	****	****	7.6	2.5
24	16.6	12.5	11.7	10.4	9.2	9.2	7.1	5.3	12.8	****	****	****	10.5	3.3
28	11.1	8.6	5.5	4.4	3.2	3.3	6.1	6.6	9.5	****	****	****	6.5	2.7
9	14.0	13.2	11.7	11.1	10.4	9.8	8.1	7.8	12.1	****	****	****	10.9	2.1

FLIGHT 2 RUN 3

POINT	REFLECTANCES FR 1	FR 2	FR 3	FR 4	FR 5	FR 6	FR 7	FR 8	FR 9	FR10	FR11	FR12	AVG	SIGMA
11	3.7	2.9	1.5	2.0	2.1	2.9	3.7	6.1	****	****	****	****	3.1	1.4
M1	4.7	4.7	4.2	4.5	3.7	4.2	5.1	6.1	****	****	****	****	4.7	0.7
33	2.1	2.1	3.5	3.8	6.1	****	****	****	****	****	****	****	3.5	1.6
25	3.0	2.0	1.6	2.2	2.9	2.2	3.8	****	****	****	****	****	2.5	0.7
14	8.4	8.1	5.3	5.7	3.8	3.2	4.2	4.9	****	****	****	****	5.4	1.8
19	4.4	3.3	2.0	0.9	0.9	1.3	2.3	3.8	****	****	****	****	2.4	1.3
M2	3.8	3.7	4.7	4.9	6.1	7.6	****	****	****	****	****	****	5.1	1.4
15	4.9	4.9	4.9	5.5	8.4	13.6	****	****	****	****	****	****	7.0	3.4
18	3.5	2.9	2.1	1.7	2.0	2.8	4.0	6.1	****	****	****	****	3.1	1.4
26	****	13.6	8.4	8.1	4.7	4.7	6.4	8.9	12.1	****	****	****	8.4	3.2
10	****	****	9.8	7.3	3.8	4.5	2.9	5.1	5.7	****	****	****	5.6	2.3
22	****	****	9.8	8.9	5.1	3.8	3.5	4.5	5.3	****	****	****	5.9	2.4
24	10.7	10.1	7.3	7.6	5.9	7.3	7.1	7.1	9.2	****	****	****	8.0	1.5
28	9.8	8.4	5.1	6.1	5.7	5.7	7.3	9.5	12.5	****	****	****	7.8	2.4
9	10.4	9.8	8.6	10.7	7.1	7.1	7.1	8.9	****	****	****	****	8.7	1.5

FLIGHT SUMMARY, FLIGHT 2

POINT	AVG	SIGMA
11	4.43	2.12
M1	4.30	0.78
33	3.42	1.75
25	4.44	2.07
14	7.77	2.96
19	3.40	2.00
M2	5.32	2.89
15	4.31	2.84
18	3.61	1.83
26	11.95	4.33
10	7.69	3.46
22	8.15	3.23
24	10.63	3.39
28	6.96	2.51
9	11.15	2.83

A P P E N D I X B

DATE MO	DA	YR	STARTING TIME	SLACK WATER	TRANSECT NUMBER
4	17	73	11 2	LOW	4

TIME HR	MIN	SEC	WATER TEMPERATURE 0.5FT D.F	3FT D.F	6FT D.F	AIR TEMP. 3FT D.F	6FT D.F	DEW PT. TEMP. D.F	SALINITY 0/00
11	2	36	56.54	56.38	56.46	67.25	66.91	66.25	2.00
11	3	12	56.71	56.54	56.62	67.50	66.75	51.90	2.03
11	3	48	56.87	56.71	56.79	67.25	66.75	52.83	2.11
11	4	24	57.12	56.96	57.04	67.16	66.42	53.24	1.98
11	5	0	57.46	57.21	57.29	67.25	66.42	53.37	2.07
11	5	36	57.62	57.46	57.46	67.25	66.50	53.10	2.03
11	6	12	57.79	57.70	57.70	67.41	66.25	52.70	2.06
11	6	48	57.95	57.87	57.79	67.16	66.58	53.77	1.90
11	7	24	58.04	57.87	57.79	67.33	66.83	52.30	2.10
11	8	0	58.04	57.87	57.62	67.08	66.83	53.10	2.05
11	8	36	58.04	57.87	57.46	67.41	67.08	52.43	2.06
11	9	12	57.95	57.79	57.70	67.75	67.33	51.64	2.05
11	9	48	57.79	57.79	57.95	67.50	67.25	52.70	2.13

DATE MO	DA	YR	STARTING TIME	SLACK WATER	TRANSECT NUMBER
4	17	73	1110	LOW	5

TIME HR	MIN	SEC	WATER TEMPERATURE 0.5FT D.F	3FT D.F	6FT D.F	AIR TEMP. 3FT D.F	6FT D.F	DEW PT. TEMP. D.F	SALINITY 0/00
11	10	32	58.78	58.54	58.62	67.58	66.91	53.64	2.04
11	11	4	58.04	57.87	57.87	67.50	66.50	53.37	2.16
11	11	36	57.46	57.46	57.46	67.58	66.50	52.57	2.05
11	12	8	57.54	57.46	57.12	67.66	66.58	52.57	2.07
11	12	40	57.70	57.54	57.21	67.75	66.00	53.64	1.95
11	13	12	57.87	57.70	57.29	67.83	66.50	52.43	1.94
11	13	44	57.79	57.54	57.46	68.00	66.58	52.83	1.96
11	14	16	57.79	57.54	57.54	68.25	67.08	52.17	2.06
11	14	48	57.79	57.62	57.62	68.08	66.66	52.83	1.99
11	15	20	57.62	57.79	57.54	68.25	67.00	52.17	1.96
11	15	52	57.62	57.46	57.46	68.16	66.83	52.57	1.95
11	16	24	57.54	57.46	57.37	68.33	66.75	52.70	2.01
11	16	56	57.46	57.37	57.37	68.25	66.66	52.70	1.98
11	17	28	57.37	57.29	57.37	68.33	66.83	52.57	1.96
11	18	0	57.12	57.04	57.12	68.41	66.91	52.04	2.05
11	18	32	56.87	56.79	56.96	68.33	67.08	53.24	1.94
11	19	4	56.87	56.71	56.87	68.75	67.50	51.90	1.99
11	19	36	57.12	57.04	57.04	68.58	68.16	50.85	2.04
11	20	8	57.54	57.46	57.37	68.58	67.33	53.10	1.97
11	20	40	57.62	57.54	57.54	68.58	66.83	53.24	1.95
11	21	12	57.46	57.21	57.21	68.91	67.08	52.43	2.06
11	21	44	56.71	56.62	56.62	68.91	67.58	51.77	2.12
11	22	16	56.71	56.54	56.46	69.00	68.41	51.77	1.93
11	22	48	56.46	56.29	56.21	70.08	68.33	51.24	2.03
11	23	20	56.29	56.13	56.04	69.25	67.91	51.64	1.94
11	23	52	56.13	55.96	55.96	69.16	67.91	51.64	2.03
11	24	24	56.21	56.04	56.04	69.25	67.33	52.70	1.95
11	24	56	56.04	55.96	55.88	69.08	68.00	51.24	1.90
11	25	28	55.96	55.79	55.54	69.08	67.83	51.51	1.95
11	26	0	55.63	55.13	55.04	69.42	68.66	50.07	1.93
11	26	32	55.54	55.21	55.21	69.25	67.75	50.98	1.94
11	27	4	55.63	55.13	55.04	69.00	66.83	51.24	1.90
11	27	36	55.63	55.38	55.21	69.00	67.50	50.85	1.98
11	28	8	55.54	55.21	55.21	69.42	68.00	50.46	1.81
11	28	40	55.21	55.04	55.13	69.00	67.33	51.38	2.03
11	29	12	54.96	54.79	54.88	69.25	67.00	50.72	1.93
11	29	44	54.96	54.96	54.96	69.00	66.91	51.90	1.93
11	30	16	55.21	55.04	55.13	69.42	68.25	50.46	1.92
11	30	48	55.13	55.04	55.13	69.42	68.58	50.59	1.90

DATE MO	DA	YR	STARTING TIME	SLACK WATER	TRANSECT NUMBER
4	17	73	1132	LOW	6

TIME HR	MIN	SEC	WATER TEMPERATURE 0.5FT D.F	3FT D.F	6FT D.F	AIR TEMP. 3FT D.F	6FT D.F	DEW PT. TEMP. D.F	SALINITY 0/00
11	32	34	55.13	55.04	55.04	69.58	68.83	51.64	2.01
11	33	8	55.21	55.04	55.13	69.58	69.33	51.77	1.89
11	33	42	55.13	55.13	55.13	69.50	68.83	52.17	1.94
11	34	16	54.88	54.96	54.79	69.33	68.50	52.57	1.91
11	34	50	55.21	54.96	55.04	69.16	68.33	52.43	1.92
11	35	24	55.29	55.04	54.96	68.91	68.08	52.97	1.89
11	35	58	54.96	54.88	54.79	69.33	68.33	52.17	1.92
11	36	32	55.21	55.21	54.96	69.08	68.00	52.70	1.94
11	37	6	55.96	55.71	55.29	69.16	68.33	52.97	1.93
11	37	40	56.04	55.71	55.38	69.08	68.08	52.83	1.94
11	38	14	56.13	55.29	55.21	69.16	68.08	52.70	2.03
11	38	48	56.04	55.54	55.38	69.08	68.16	52.97	1.93
11	39	22	56.21	55.71	55.46	69.08	68.08	52.97	1.87
11	39	56	56.29	55.71	55.54	69.33	68.41	52.57	1.85
11	40	30	56.46	56.13	55.71	69.16	68.41	52.17	1.92
11	41	4	56.71	56.21	55.96	68.91	68.41	52.70	2.02
11	41	38	57.04	56.54	56.04	69.33	68.58	52.04	2.01
11	42	12	57.46	57.04	56.13	69.50	68.08	52.43	1.89
11	42	46	57.79	56.79	56.21	69.58	68.08	52.57	1.89
11	43	20	57.70	57.04	56.21	69.50	68.08	52.43	1.89
11	43	54	57.70	56.87	56.38	69.58	68.50	53.37	1.94
11	44	28	57.87	57.12	56.71	69.33	68.50	53.24	1.93
11	45	2	57.87	57.37	56.79	69.25	68.08	53.37	1.88
11	45	36	57.79	57.37	56.62	69.08	67.91	53.64	1.94
11	46	10	57.54	57.21	56.54	69.08	67.91	53.50	1.93
11	46	44	57.37	57.04	56.29	69.00	68.00	53.24	1.93
11	47	18	57.37	57.04	56.04	69.00	67.91	52.97	1.95
11	47	52	57.29	57.12	56.54	68.83	67.25	53.37	1.92

DATE MO	DA	YR	STARTING TIME	SLACK WATER	TRANSECT NUMBER
4	17	73	1149	LOW	7

TIME			WATER	TEMPERATURE		AIR	TEMP.	DEW PT.	SALINITY
			0.5FT	3FT	6FT	3FT	6FT	TEMP.	0/00
HR	MIN	SEC	D.F	D.F	D.F	D.F	D.F	D.F	
11	49	30	56.96	56.87	56.29	69.33	68.41	51.51	1.98
11	50	0	57.04	56.96	55.88	69.67	68.83	51.11	2.03
11	50	30	57.04	56.46	55.71	69.25	68.16	52.04	1.88
11	51	0	56.96	56.38	55.63	69.25	67.41	52.97	1.88
11	51	30	56.79	56.62	55.46	69.25	67.75	52.17	1.95
11	52	0	56.71	56.46	55.21	69.16	68.08	52.04	1.92
11	52	30	56.29	56.13	55.04	69.33	67.91	51.90	1.89
11	53	0	55.96	55.79	54.79	69.42	67.83	52.57	1.95
11	53	30	56.46	56.04	54.54	69.00	67.75	52.83	1.93
11	54	0	56.46	55.38	54.46	69.25	67.58	51.51	1.92
11	54	30	54.54	54.46	54.46	69.42	68.08	51.38	1.91
11	55	0	54.54	54.46	54.46	69.67	68.66	50.98	1.92
11	55	30	54.63	54.71	54.71	69.92	68.25	51.51	1.88
11	56	0	57.04	56.71	55.04	69.67	68.66	52.17	1.91
11	56	30	57.70	57.12	55.21	69.58	68.16	53.10	1.89
11	57	0	58.12	57.54	55.46	69.67	68.91	51.90	1.89
11	57	30	58.04	57.70	56.04	70.08	69.00	51.24	1.90
11	58	0	58.20	57.70	56.79	69.92	69.16	51.51	1.97
11	58	30	58.29	57.70	56.87	70.00	69.00	51.77	1.99
11	59	0	58.54	58.04	56.87	70.17	68.83	51.24	1.91
11	59	30	58.78	58.37	56.71	70.33	69.50	51.11	1.92
12	0	0	58.87	58.37	56.62	70.17	69.25	51.38	1.65
12	0	30	58.78	58.12	56.29	69.83	68.33	51.90	1.65
12	1	0	58.37	57.79	56.04	69.83	68.58	51.64	1.65
12	1	30	57.62	57.12	55.79	69.83	68.75	51.24	1.65
12	2	0	56.79	56.71	55.29	69.58	68.41	52.04	1.65
12	2	30	55.46	55.21	55.13	69.75	68.66	51.38	1.65

DATE MO	DA	YR	STARTING TIME	SLACK WATER	TRANSECT NUMBER
4	17	73	12 3	LOW	8

TIME HR	MIN	SEC	WATER TEMPERATURE 0.5FT D.F	3FT D.F	6FT D.F	AIR TEMP. 3FT D.F	6FT D.F	DEW PT. TEMP. D.F	SALINITY 0/00
12	3	20	56.13	56.13	55.21	70.25	69.67	50.07	1.65
12	3	40	57.54	57.04	55.54	70.42	69.67	51.38	1.65
12	4	0	58.20	57.54	55.63	70.33	69.58	51.64	1.65
12	4	20	58.78	57.87	55.88	70.17	69.25	52.70	1.65
12	4	40	58.87	57.79	56.04	70.50	69.75	51.24	1.65
12	5	0	58.95	58.20	56.38	68.33	69.75	52.43	1.65
12	5	20	58.95	58.37	56.29	70.59	70.25	51.51	1.65
12	5	40	58.62	58.29	56.54	70.50	70.25	51.90	1.65
12	6	0	58.29	57.46	56.62	70.75	70.50	50.72	1.65
12	6	20	58.37	57.95	56.13	70.84	70.25	51.24	1.65
12	6	40	58.20	57.87	56.62	70.92	70.25	51.51	1.65
12	7	0	58.20	57.79	56.29	71.00	70.42	51.38	1.65
12	7	20	57.87	57.54	56.29	70.92	70.25	52.04	1.65
12	7	40	55.21	54.79	54.71	70.92	70.25	52.04	1.65
12	8	0	54.88	54.71	54.71	71.00	70.25	52.30	1.65
12	8	20	54.88	54.71	54.71	71.00	70.17	51.90	1.65
12	8	40	54.88	54.79	55.21	70.92	70.08	51.90	1.65
12	9	0	56.46	55.88	55.13	71.17	70.00	51.90	1.65
12	9	20	56.13	55.38	55.04	70.92	70.08	51.64	1.65
12	9	40	55.79	55.38	55.21	71.26	70.08	51.51	1.65
12	10	0	55.79	55.71	55.29	71.26	70.08	51.51	1.65
12	10	20	55.88	55.29	55.13	71.17	70.17	51.11	1.65
12	10	40	55.79	55.71	55.63	71.34	70.25	51.11	1.65
12	11	0	55.71	55.63	55.71	71.09	70.08	52.04	1.65

R E F E R E N C E S

Boon, J.D., III, 1973. Sediment transport processes in a salt marsh drainage system. Unpublished Ph.D. dissertation, College of William and Mary, Williamsburg, Virginia.

Borgese, D., G. Dinelli, F. Parrini, D.T. Hodder, D.D. Steller, 1972. Isothermal Mapping of Temperature Patterns from Thermal Discharges in Italian Coastal Waters. Proceedings of the Eighth International Symposium on Remote Sensing of Environment, Vol. I.

Byrne, R.J., P. Bullock and D.G. Tyler, 1973. Response Characteristics of a tidal inlet: a case study, Proc. of the 2nd Internat'l. Estuarine Res. Conf., Myrtle Beach, S.C. (in press).

Egan, Walter G. and Malcolm E. Hair, 1971. Automated Delineation of Wetlands in Photographic Remote Sensing. Proceedings of the Seventh International Symposium on Remote Sensing of the Environment, Vol. III.

Egbert, Dwight D. and Fawwaz, T. Ulaby, 1972. Effect of Angles on Reflectivity. Photogrammetric Engineering, Vol. 38, No. 6.

Gallagher, John L., Robert J. Reimold, and Donald E. Thompson, 1972. Remote Sensing and Salt Marsh Productivity. Proceedings of the 38th Annual Meeting, American Society of Photogrammetry.

Gallagher, John L., Robert J. Reimold, and Donald E. Thompson, 1972. A Comparison of Four Remote Sensing Media for Assessing Salt Marsh Primary Productivity. Manuscript.

Gordon, Hayden H., John C. Munday, Michael E. Penney, 1971. Remote Sensing Applications in Marine Science Programs at VIMS. First Year Report. NASA Contract NAS 6-1902.

Gordon, Hayden H., Michael E. Penney, 1972. Remote Sensing Applications in Marine Science Programs at VIMS. Second Year Report. NASA Contract NAS 6-1902.

Hoffer, Roger M., Roger A. Holmes and J. Ralph Shay, 1966. Vegetative soil, and photographic factors affecting tone in Agricultural Remote Multispectral Sensing. Proceedings of the Fourth International Symposium on Remote Sensing of Environment. University of Michigan, Ann Arbor, Michigan.

Holter, Marvin R., Sol Nudelman, Gwynn H. Suits, William L. Wolfe, George J. Zissis, 1962. Fundamentals of Infrared Technology. The Macmillan Company, New York. 442 pp.

Klemas, V., F.C. Daiber, D.S. Bartlett, O.W. Crichton and A.G. Fornes, 1973. Coastal Vegetation of Delaware. College of Marine Studies, University of Delaware.

Leendertse, J.J., R.C. Alexander and Shioa, Kung Liu, 1973. A three-dimensional model for estuaries and coastal seas: Vol. 1, Principles of computation. Rand Corp. R-1417, Dec. 57 pp.

Masry, S.E., J.G. Gibbons, 1973. Distortion and Rectification of IR. Photogrammetric Engineering, Vol. XXXIX, No. 8.

Mota Oliveira, I.B., 1970. Natural flushing ability of tidal inlets, Proc. 12 Conference Coastal Engineering, 1827-1845.

O'Brien, M.P., 1969. Dynamics of tidal inlets. In Coastal Lagoons, a Symposium, 397-407 (ed. Castanares, A.A., and Phleger, F.B.) Universidad Nacional Autonoma de Mexico.

O'Brien, M.P. and R.R. Clark, 1973. Hydraulic constants of tidal entrances 1: Data from NOS tide tables, current tables and navigation charts. Univ. of Florida Coastal and Oceanographic Engineering Laboratory Tech. Report No. 21, Nov. 50 pp.

Reimold, Robert J., 1971. Remote Sensing of Salt Marsh Productivity. Proceedings of the Third Biennian Workshop on Color Aerial Photography in the Plant Sciences.

Sabins, Floyd F., Jr., 1973. Recording and Processing Thermal IR Imagery. Photogrammetric Engineering, Vol. XXXIX, No. 8.

Shearls, E.A., S.N. Chia, W.J. Hargis, Jr., C.S. Fang, and R.N. Lobecker, 1973. Thermal Effects of the Surry Nuclear Power Plant on the James River, Virginia. VIMS Sepcial Report No. 33.

Silvestro, Frank B., 1968. Multispectral Photographic Determination of Reflectance. Thirty-eighth Annual Meeting, American Society of Photogrammetry.

Steiner, Dieter and Harold Haefner, 1965. Tone Distortion for Automated Interpretation. Photogrammetric Engineering, Vol. 31, No. 2.

Suits, Gwynn H., 1972. The Calculation of the Directional Reflectance of a Vegetative Canopy. Remote Sensing of Environment, Vol. 2.

Suits, Gwynn H., 1972. The Cause of Azimuthal Variations in Directional Reflectance of Vegetative Canopies. Remote Sensing of Environment, Vol. 2.

Wobber, Frank J. and Richard R. Anderson, 1972. Operational Wetlands Mapping using Multiband Aerial Photography. Coastal Mapping Symposium. American Society of Photogrammetry.